SUPPLEMENTARY INFORMATION

Systematic identification of genomic markers of drug sensitivity in cancer cells

Mathew J. Garnett[1,*], Elena J. Edelman[2,*], Sonja J. Heidorn[1,*], Chris D. Greenman[1†‡], Anahita Dastur[2], King Wai Lau[1], Patricia Greninger[2], I. Richard Thompson[1], Xi Luo[2], Jorge Soares[1], Qingsong Liu[3,4], Francesco Iorio[1,5], Didier Surdez[6], Li Chen[2], Randy J. Milano[2], Graham R. Bignell[1], Ah T. Tam[2], Helen Davies[1], Jesse A. Stevenson[2], Syd Barthorpe[1], Stephen R. Lutz[2], Fiona Kogera[1], Karl Lawrence[1], Anne McLaren-Douglas[1], Xeni Mitropoulos[2], Tatiana Mironenko[1], Helen Thi[2], Laura Richardson[1], Wenjun Zhou[3,4], Frances Jewitt[1], Tinghu Zhang[3,4], Patrick O'Brien[1], Jessica L. Boisvert[2], Stacey Price[1], Wooyoung Hur[3,4], Wanjuan Yang[1], Xianming Deng[3,4], Adam Butler[1], Hwan Geun Choi[3,4], Jae Won Chang[3,4], Jose Baselga[2], Ivan Stamenkovic[7], Jeffrey A. Engelman[2], Sreenath V. Sharma[2,§], Olivier Delattre[6], Julio Saez-Rodriguez[5], Nathanael S. Gray[3,4], Jeffrey Settleman[2], P. Andrew Futreal[1], Daniel A. Haber[2, 8], Michael R. Stratton[1], Sridhar Ramaswamy[2], Ultan McDermott[1], Cyril H. Benes[2].

[1]Cancer Genome Project, Wellcome Trust Sanger Institute, Hinxton CB10 1SA, UK.

[2]Massachusetts General Hospital Cancer Center, Harvard Medical School, Charlestown MA 02129, USA

[3]Department of Cancer Biology, Dana Farber Cancer Institute, 44 Binney Street, Boston MA 02115, USA

[4]Department of Biological Chemistry and Molecular Pharmacology, Harvard Medical School, 250 Longwood Ave. Boston MA 02115, USA

[5]EMBL-EBI, Wellcome Trust Genome Campus, Cambridge CB10 1SD, UK

[6]Laboratoire de génétique et biologie des cancers, Institut Curie, 75248 Paris, Cedex 05, France

[7]Division of Experimental Pathology, Institute of Pathology, Centre Hospitalier Universitaire Vaudois (CHUV), University of Lausanne, Lausanne, Switzerland.

[8]Howard Hughes Medical Institute, Chevy Chase MD 20815, USA

†Present Address: Department of Computing, University of East Anglia, Norwich NR4 7TJ, UK.

‡Present Address: The Genome Analysis Centre, Norwich Research Park, Norwich NR4 7UH, UK

[§]Present address: Oncology Drug Discovery, Novartis Institutes for Biomedical Research, 250 Massachusetts Avenue, Cambridge, MA 02139

*These authors contributed equally to this work.

Correspondence and requests for material should be addressed to U.M (um1@sanger.ac.uk) or C.B. (cbenes@partners.org)

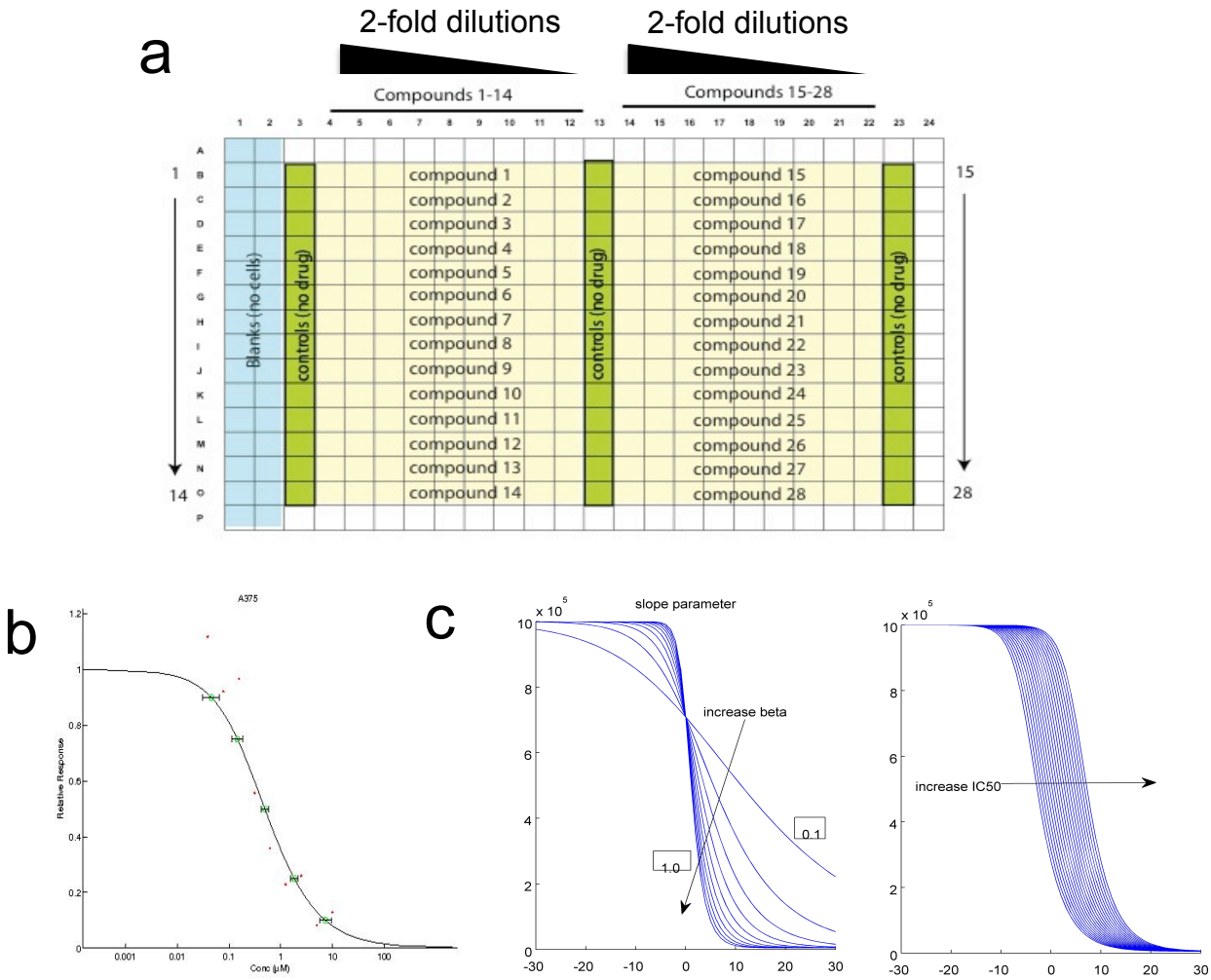

Supplementary Figure 1: Screening format and curve-fitting algorithm. **a**, A schematic diagram of a typical 384-well screening plate. A single cell line is used on each plate and treated with 28 different drugs over a 9-pt, 256-fold concentration range. Wells with no cells (blanks) and untreated wells (controls) are used as controls on each plate. **b**, An example of curve-fitting of drug sensitivity data to generate a multi-parameter description of drug response. Red circles are normalized screening data and the curve fit is shown. Green circles represent IC_{10}, IC_{25}, IC_{50}, IC_{75} and IC_{90} values and error bars are confidence intervals. **c**, Representations of output parameters calculated from the curve-fitting algorithm. The slope parameter (beta) and IC_{50} value from the dose-response curve are shown.

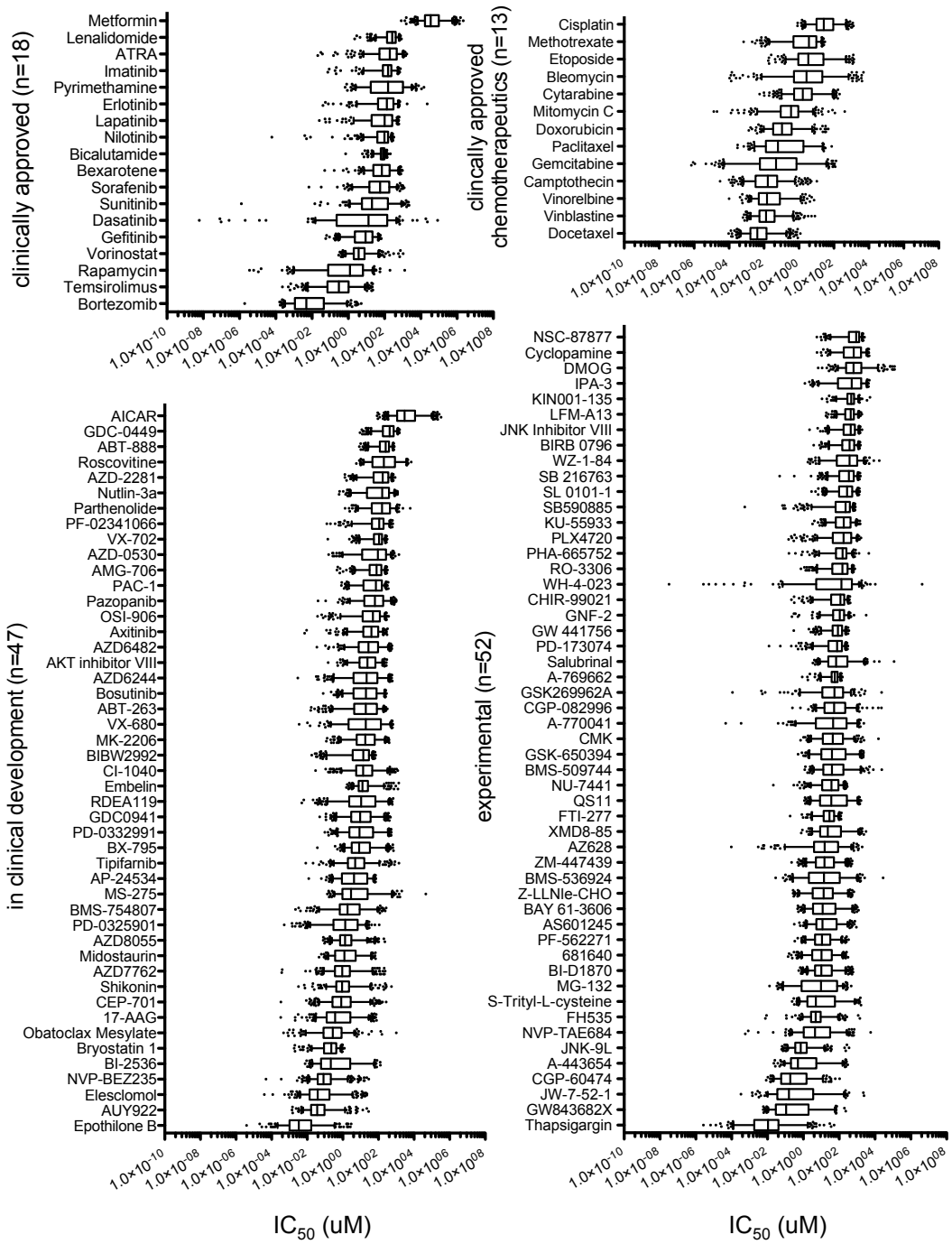

Supplementary Figure 2: Cell line sensitivity across the drug collection. Drugs are classified as clinically approved, clinically approved chemotherapeutics, in clinical development or experimental. For each drug the range of cell line IC_{50} values is represented as a box and whisker plot. The median IC_{50}, interquartile ranges, and 95% confidence intervals are shown for each drug. Outlier cell line IC_{50}s are indicated by black dots.

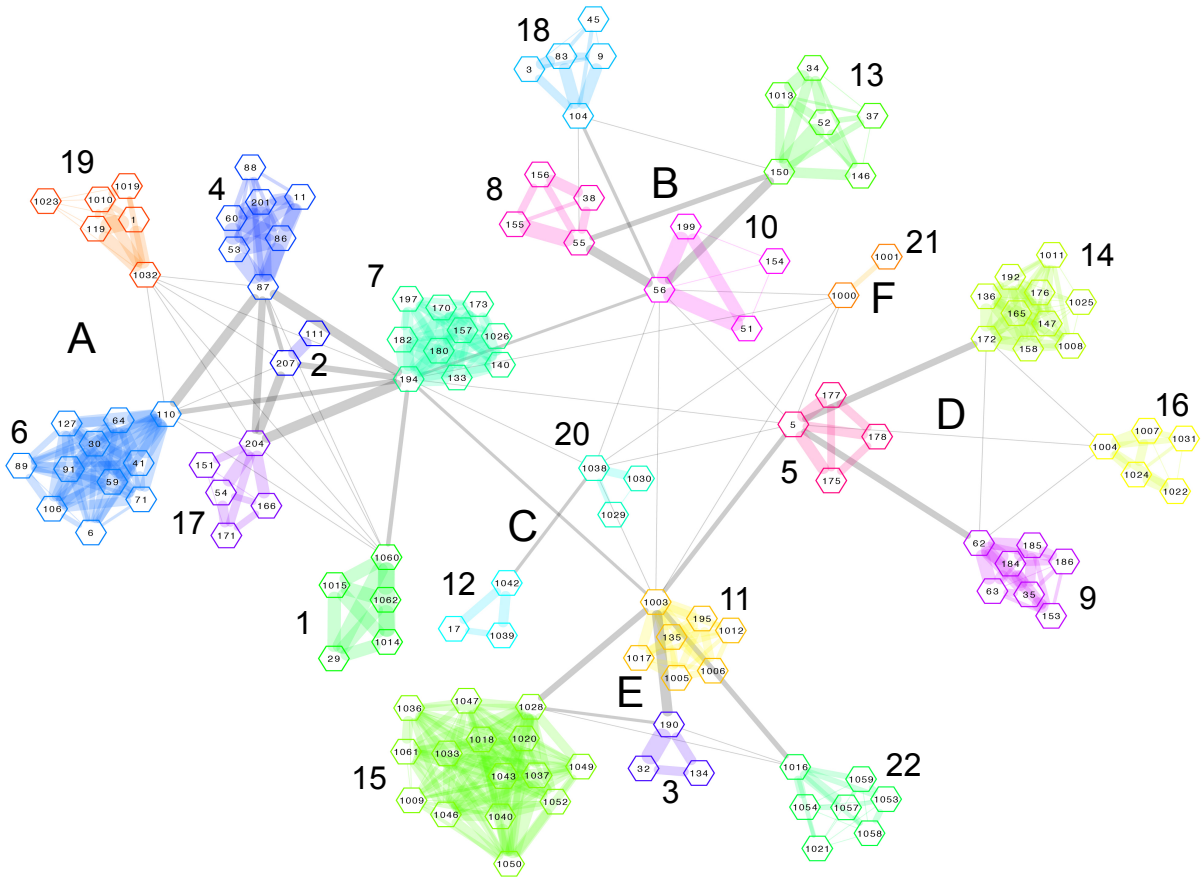

Supplementary Figure 3: Clustering of drugs based on IC_{50} values. A network visualization of drug similarity based on cell line IC_{50} values. Drugs are clustered in 22 communities (1-22) and 6 “communities of communities” (A-F, rich clubs) dependent on their intra and inter cluster correlations, respectively. An ID number identifies individual drugs and the thickness of an edge is proportional to the similarity of the connected nodes and different colors indicate different clusters. Node positions roughly reflect drug similarities (i.e. the closer two nodes are the more correlated the IC_{50} patterns of the corresponding drugs are) and have been computed through the “spring-embedding” algorithm for network layout.

C	total Avg Corr	odd Ratio	Drug id	Avg Corr	Drug Generic Name	Drug Target
1	0.7338	5.8277	1060	0.8162	PD-0325901 *	MEK1/2
			1062	0.7999	AZD6244	MEK1/2
			1014	0.7961	RDEA119	MEK1/2
			29	0.7644	AZ628	BRAF
			1015	0.7585	CI-1040	MEK1/2
2	0.6960	5.5745	207	0.8480	AS601245 *	JNK
			111	0.8480	Salubrinal	GADD34-PP1C phosphatase
3	0.6600	5.1446	190	0.8164	Bleomycin *	DNA damage
			32	0.8077	VX-680	Aurora A/B/C, FLT3, ABL1, JAK2,
			134	0.6958	Etoposide	TOP2
4	0.6409	5.0275	87	0.7933	GW843682X *	PLK1
			60	0.7861	BI-2536	PLK1/2/3
			86	0.7402	A-443654	AKT1/2/3
			201	0.7302	Epothilone B	Microtubules
			53	0.7286	CGP-60474	CDK1/2/5/7/9
			11	0.6501	Paclitaxel	Microtubules
			88	0.4169	MS-275	HDAC
5	0.5500	4.3118	5	0.7202	Sunitinib *	PDGFRA, PDGFRB, KDR, KIT, FLT3
			177	0.6586	GSK-650394	SGK3
			175	0.6372	PAC-1	CASP3 activator
			178	0.6339	BAY 61-3606	SYK
6	0.5327	4.1633	110	0.6801	Roscovitine *	CDKs
			59	0.6578	WZ-1-84	BMX
			91	0.6259	KIN001-135	IKKe
			41	0.6087	S-Trityl-L-cysteine	KIF11
			30	0.6008	Sorafenib	PDGFRA, PDGFRB, KDR, KIT, FLT3
			106	0.5917	XMD8-85	ERK5
			64	0.5879	CMK	RSK
			127	0.5824	GSK269962A	ROCK
			71	0.5208	Pyrimethamine	STAT3
			89	0.4621	Parthenolide	NFkappaB
			6	0.4089	PHA-665752	MET
7	0.5266	4.1296	194	0.6685	NVP-AUY922 *	HSP90
			180	0.6399	Thapsigargin	ATPase, Ca++ transporting, cardiac muscle, slow twitch 2
			157	0.6184	JNK-9L	JNK
			182	0.6082	Obatoclax Mesylate	BCL-2, BCL-XL, MCL-1
			133	0.5978	Doxorubicin	DNA intercalating
			140	0.5865	Vinorelbine	Microtubules
			170	0.5530	Shikonin	unknown
			173	0.5296	FH535	unknown
			197	0.4869	Bryostatin 1	PRKC
			1026	0.4505	17-AAG	HSP90
8	0.5182	4.0438	55	0.6868	A-770041 *	SRC family
			155	0.6437	AP-24534	ABL
			156	0.6259	AZD6482	PI3Kb
			38	0.5982	AZD-0530	SRC, ABL1
9	0.5055	3.9489	62	0.6946	BMS-536924 *	IGF-1R
			184	0.6846	BMS-754807	IGF1R
			35	0.6378	NVP-TAE684	ALK
			185	0.5832	OSI-906	IFG1R
			153	0.5137	Midostaurin	KIT
			63	0.4895	BMS-509744	ITK
			186	0.4296	Bexarotene	Retinioic acid X family agonist
10	0.4931	3.8986	56	0.7207	WH-4-023 *	SRC family
			51	0.6816	Dasatinib	ABL, SRC, KIT, PDGFR
			199	0.6571	Pazopanib	VEGFR, PDGFRA, PDGFRB, KIT
			154	0.4200	CHIR-99021	GSK3b
11	0.4826	3.7883	1003	0.6594	Camptothecin *	TOP1
			195	0.6083	Camptothecin	TOP1
			135	0.5947	Gemcitabine	DNA replication
			1006	0.5309	Cytarabine	Inhibits DNA synthesis
			1017	0.5292	AZD-2281	PARP1/2
			1005	0.5141	Cisplatin	DNA crosslinking
			1012	0.4587	Vorinostat	HDAC inhibitor Class I, IIa, IIb, IV
12	0.4838	3.7723	1042	0.6823	BIRB 0796 *	p38, JNK2
			1039	0.6489	SL 0101-1	RSK, AURKB, PIM3
			17	0.6364	Cyclopamine	SMO
13	0.4602	3.6161	150	0.6569	Bicalutamide *	Androgen receptor
			52	0.6457	GNF-2	BCR-ABL
			34	0.5551	Imatinib	ABL, KIT, PDGFR
			1013	0.5312	Nilotinib	ABL
			146	0.4924	A-769662	AMPK
			37	0.4195	PF-2341066	MET, ALK
14	0.4362	3.4325	172	0.5933	Embelin *	XIAP
			147	0.5606	NSC-87877	SHP1/2
			165	0.5532	DMOG	Prolyl-4-Hydroxylase
			176	0.5527	IPA-3	PAK
			158	0.5477	PF-562271	FAK
			136	0.5239	Mitomycin	DNA crosslinker
			192	0.4787	LFM-A13	BTK
			1008	0.4575	Methotrexate	Dihydrofolate reductase (DHFR)
			1011	0.3896	ABT-263	BCL2, BCL-XL, BCL-W
			1025	0.2685	SB 216763	GSKa/b
15	0.4296	3.3583	1028	0.5844	VX-702 *	p38 MAPK
			1043	0.5728	JNK Inhibitor VIII	JNK
			1046	0.5212	681640	WEE1, CHK1
			1037	0.5187	BX-795	TBK1, PDK1, IKK, AURKB/C
			1040	0.5150	BI-D1870	RSK1/2/3/5/, PLK1, AURKB
			1050	0.5146	ZM-447439	AURKB
			1018	0.4974	ABT-888	PARP1/2
			1061	0.4737	SB590885	BRAF
			1020	0.4736	Lenalidomide	TNF alpha
			1049	0.4250	PD-173074	FGFR1/3
			1052	0.4221	RO-3306	CDK1
			1036	0.4159	PLX4720	BRAF
			1047	0.3976	Nutlin-3a	MDM2
			1033	0.3718	GDC-0449	SMO
			1009	0.3112	ATRA	Retinoic acid and retinoid X receptor agonist
16	0.4252	3.3359	1004	0.6108	Vinblastin *	Microtubules
			1024	0.5860	CEP-701	FLT3, JAK2, TrkA, RET
			1007	0.5537	Docetaxel	Microtubules
			1022	0.5039	AZD7762	CHK1/2
			1031	0.4464	Elesclomol	HSP70
17	0.4215	3.3315	204	0.6454	Tipifarnib *	Farnesyl-transferase
			54	0.5818	CGP-082996	CDK4
			166	0.5250	FTI-277	Farnesyl transferase
			171	0.5186	AKT inhibitor VIII	AKT1/2
			151	0.4150	QS11	ARFGAP
18	0.4095	3.2365	104	0.6076	Bortezomib *	Proteasome
			83	0.6004	JW-7-52-1	MTOR
			3	0.5175	Rapamycin	MTOR
			9	0.5172	MG-132	Proteasome
			45	0.3952	Z-LLNle-CHO	g-secretase
19	0.3659	2.8674	1032	0.5838	BIBW2992 *	EGFR, ERBB2
			1	0.5620	Erlotinib	EGFR
			119	0.5479	Lapatinib	EGFR, ERBB2
			1010	0.4803	Gefitinib	EGFR
			1019	0.4036	Bosutinib	SRC, ABL, TEC
			1023	0.2519	GW 441756	NTRK1
20	0.3555	2.7617	1038	0.6160	NU-7441 *	DNAPK
			1030	0.5744	KU-55933	ATM
			1029	0.5206	AMG-706	VEGFR, RET, c-KIT, PDGFR
21	0.3465	2.7612	1000	0.6733	Metformin *	AMPK
			1001	0.6733	AICAR	AMPK
22	0.2936	2.2959	1016	0.4957	Temsirolimus *	mTOR
			1057	0.4629	NVP-BEZ235	PI3K Class 1 and mTORC1/2
			1053	0.3970	MK-2206	AKT1/2
			1054	0.3943	PD-0332991	CDK4/6
			1058	0.3583	GDC0941	PI3K class 1
			1059	0.3444	AZD8055	mTORC1/2
			1021	0.3093	Axitinib	PDGFR, KIT, VEGFR

* community exemplars

Supplementary Table 1: Intra-cluster drug correlations. Communities are sorted according to the intra-community similarity score and drugs are sorted according to their similarity to the exemplar (*) within each community. The intra-community similarity score is calculated as an odds ratio (see Supplementary Methods for more detail). As an experimental control the drug camptothecin was screened twice across the cell line collection and the resulting drug sensitivity data were correlative with both datasets clustering together in community 11 (C11). Drugs with overlapping reported targets such as multiple MEK1/2 (C1), EGFR/ERBB2 (C19) and IGFR1 (C9) inhibitors frequently clustered together demonstrating overlapping sensitivity profiles across the cell line panel. In some instances however this was not the case (e.g. SRC inhibitors, C8, C10 and C19) indicating perhaps differences in the modes of action and target selectivity of these drugs. The community clusters (C) correspond to the numbering in Supplementary Figure 3.

	1	2	4	6	7	17	19	8	10	13	18	12	20	5	9	14	16	3	11	15	22	21	
1				0.2395	0.3477									-0.8813		-0.1916						-0.1384	
2			0.2643		0.2544	0.2856												0.3422					
4		0.2643		0.3428	0.4440	0.4665		0.2756							0.3163	-0.9376		0.3928	0.2496				
6	0.2395		0.3428		0.3112	0.2756		0.2434	-0.1268		-0.2788			-0.9193	0.2385	-0.2777			-0.1778	-0.4549			A
7	0.3477	0.2544	0.4440	0.3112		0.3194		0.2657						-0.5656	0.2349	-0.3827		0.3265				-0.1291	
17		0.2856	0.4665	0.2756	0.3194			0.2778								-0.6515		0.3382					
19									-0.5179		-0.1130			-0.4989	-0.2494	-0.3555				-0.1846			
8			0.2756	0.2434	0.2657	0.2778			0.4260	0.2723						-0.1537						-0.5998	
10				-0.1268			-0.5179	0.4260		0.2947	0.2415												
13								0.2723	0.2947														B
18				-0.2788			-0.1130		0.2415													-0.1468	
12													0.2812										
20												0.2812											C
5	-0.8813			-0.9193	-0.5656		-0.4989								0.2664	0.4177		0.3689	0.3544				
9			0.3163	0.2385	0.2349		-0.2494							0.2664					0.2365			-0.2956	
14	-0.1916		-0.9376	-0.2777	-0.3827	-0.6515	-0.3555	-0.1537						0.4177					0.1990			0.3117	D
16																			0.2698	-0.6500	0.2296		
3		0.3422	0.3928		0.3265	0.3382								0.3689					0.4197				
11			0.2496	-0.1778										0.3544	0.2365	0.1990	0.2698	0.4197		0.2762			
15				-0.4549			-0.1846										-0.6500		0.2762		-0.3716		E
22																	0.2296			-0.3716			
21	-0.1384				-0.1291			-0.5998			-0.1468				-0.2956	0.3117							F
	A							B				C		D				E				F	

Supplementary Table 2: Cluster-to-cluster similarity scores and rich-club compositions. The inter-cluster similarity score is provided for each pair of communities and quantifies the extent of their similarity. Green values indicates positive similarities (correlations) while red values indicate "negative" ones (anti-correlations). Only significant values ($P < 0.05$) were included and communities (1 - 22) were grouped to reflect the rich-club compositions (A - F).

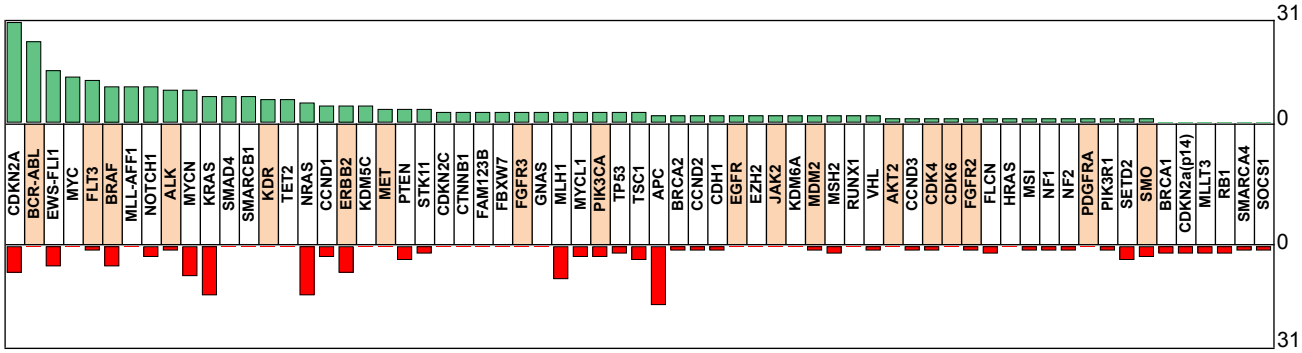

Supplementary Figure 4: The majority of cancer genes are associated with drug response. The number of statistically significant sensitizing (green bars) or resistance (red bars) associations identified by MANOVA for each cancer gene. Genes that are reported to be the direct target of a screening drug are coloured. The following genes were analysed but were not associated with drug response: *IDH1*, *MAP2K4*, *KIT*, *MSH6*. Drug response was also correlated with microsatellite instability (MSI) status.

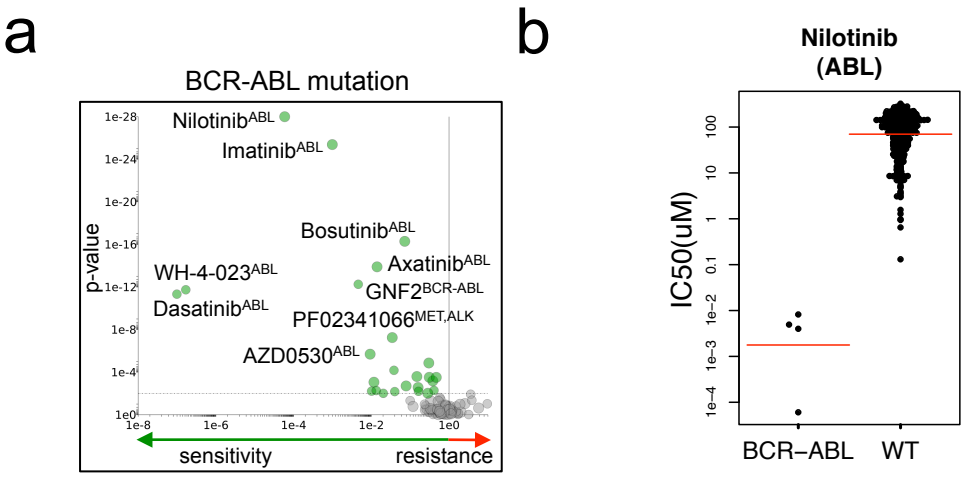

Supplementary Figure 5: The *BCR-ABL* rearrangement is associated with sensitivity to multiple ABL inhibitors. **a**, A gene-specific volcano plot from the MANOVA showing the magnitude (effect; x-axis) and significance (p-value; inverted y-axis) of drug sensitivity associated with *BCR-ABL* mutations in cancer cell lines. Each circle represents a single drug interaction and for selected associations the drug name and therapeutic drug target(s) (in superscript) are indicated. A horizontal dashed line indicates the threshold of statistical significance (0.2 FDR, $P < 0.0099$) and significant associations with drug sensitivity are coloured green. *BCR-ABL* was not associated with drug resistance. For clarity, the p-value for nilotinib ($P = 2.54 \times 10^{-65}$) has been capped at 1×10^{-28}. **b**, A scatter plot of *BCR-ABL* mutated or wild-type (WT) cell line IC_{50} values for nilotinib. Each circle represents the IC_{50} of one cell line on a log scale and the red bar is the geometric mean.

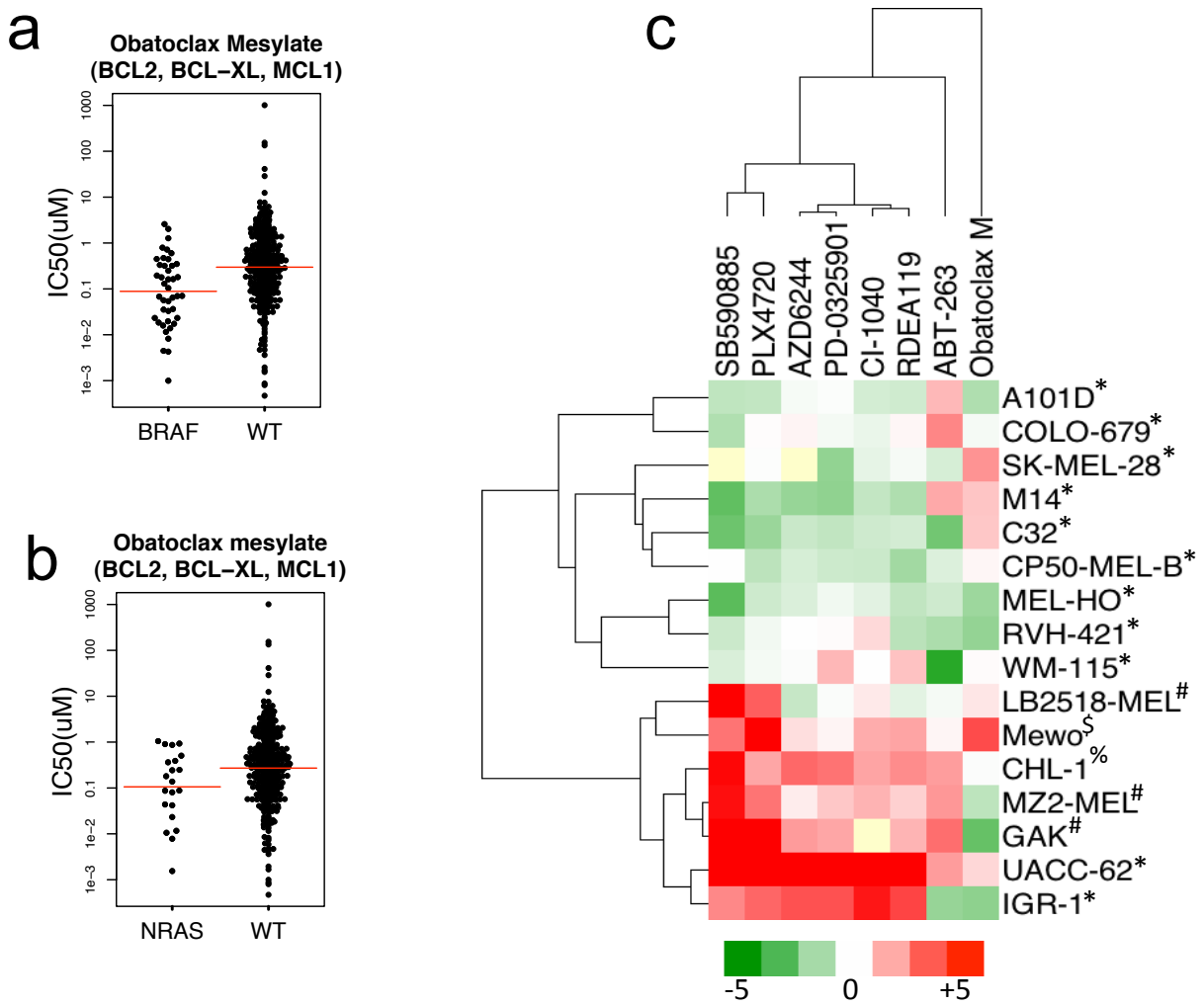

Supplementary Figure 6: ***BRAF* and *NRAS* mutations are markers of melanoma sensitivity to obatoclax mesylate**. **a** and **b**, Scatter plots from screening data of obatoclax mesylate IC_{50} values of **a**, BRAF or **b**, NRAS mutated versus wild-type (WT) cell lines. The p-values from the MANOVA analysis for these associations are $P = 1.4 \times 10^{-4}$ and $P = 0.0055$ for *BRAF* and *NRAS*, respectively. Each circle represents the IC_{50} of one cell line on a log scale and the red bar is the geometric mean. **c**, A heatmap comparing sensitivity of melanoma cell lines to obatoclax mesylate, ABT-263, BRAF inhibitors (PLX4720, SB590885), MEK1/2 inhibitors (AZD6244, PD-0325901, CI-1040, RDEA119). Sensitivity to obatoclax is not correlated with sensitivity to MEK or BRAF inhibitors. The colour scale corresponds to median centered natural log (IC_{50}) values. Mutational status is indicated as follows: *, *BRAF* V600; #, *NRAS*; $, *NF1;* %, *KRAS* amplified.

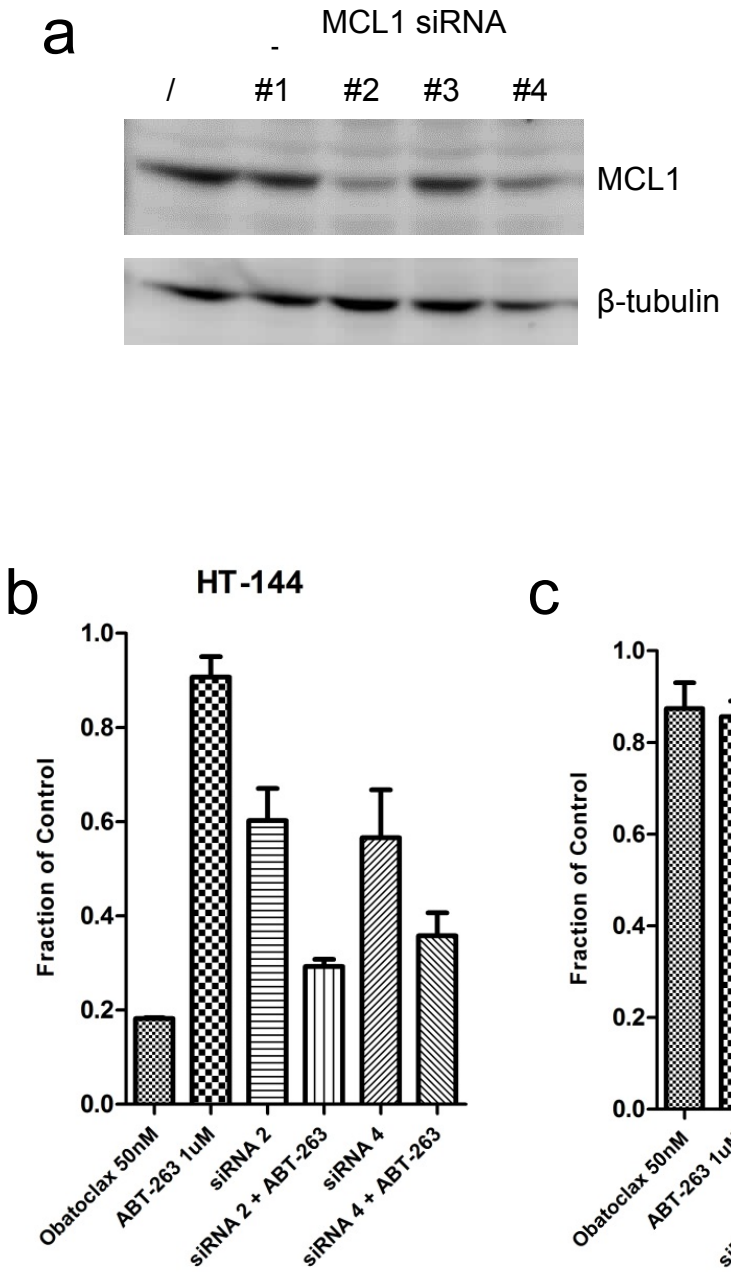

Supplementary Figure 7: MCL1 knockdown sensitises melanoma cells to ABT-263. a, Western blot of MCL1 protein levels in mock transfected cells or following 72 hr knockdown with multiple MCL1 siRNA. siRNA #2 and #4 gave the most efficient knockdown and were selected for subsequent cell viability assays. **b** and **c**, Effect on the cell viability of the *BRAF* (V600E) mutant HT-144 melanoma cell line after 72 hour treatment with obatoclax (50 nM), or ABT-263 (1 uM) alone or together with 40 nM MCL1 siRNA. The lung cancer cell line A549 which is wild-type for *BRAF* was used as negative control. Cell viability was assayed in triplicate and error bars represent standard deviations.

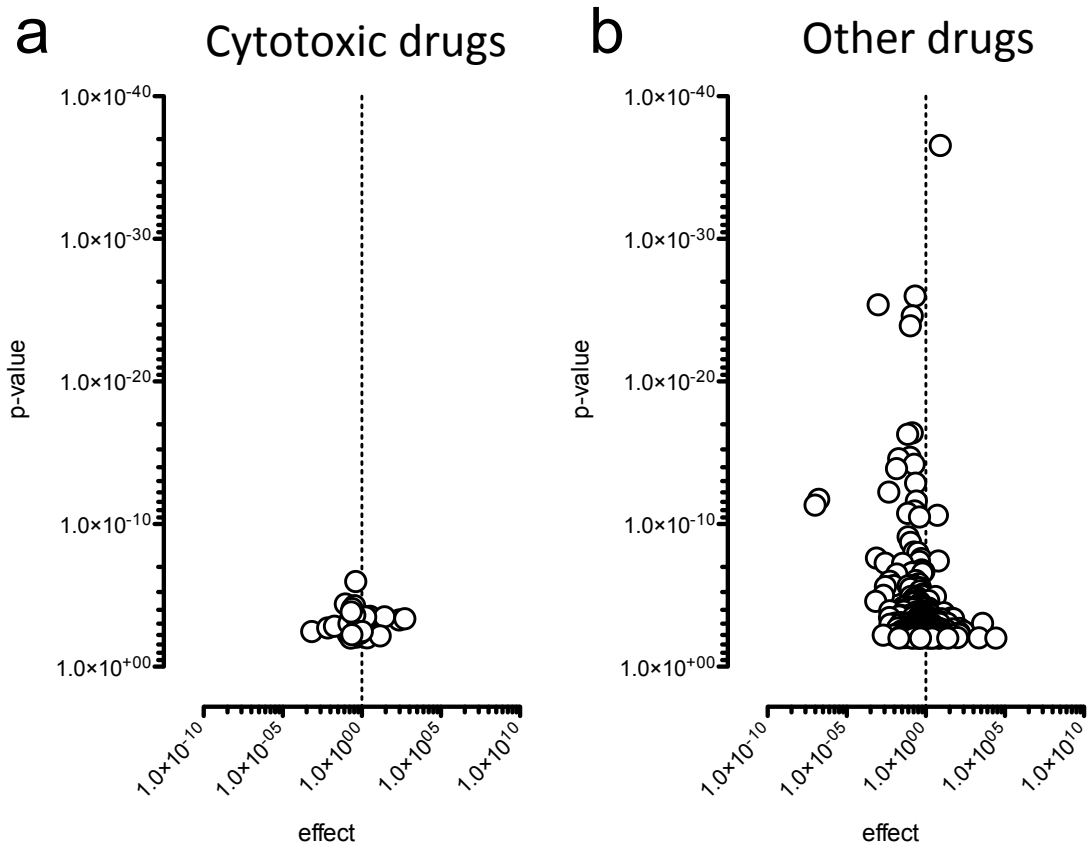

Supplementary Figure 8: **Cytotoxic chemotherapeutic drugs were not associated with highly significant genomic correlations**. Volcano plots showing the effect size (x-axis) and p-value (y-axis, inverted scale) of statistically significant associations identified by the MANOVA. **a**, Cytotoxic drugs (*n*= 13) were correlated with 41 associations and **b** the remaining drugs (*n* = 117) with 407 associations. For clarity the association between nilotinib and *BCR-ABL* ($P = 2.45 \times 10^{-65}$) has been excluded from **b**.

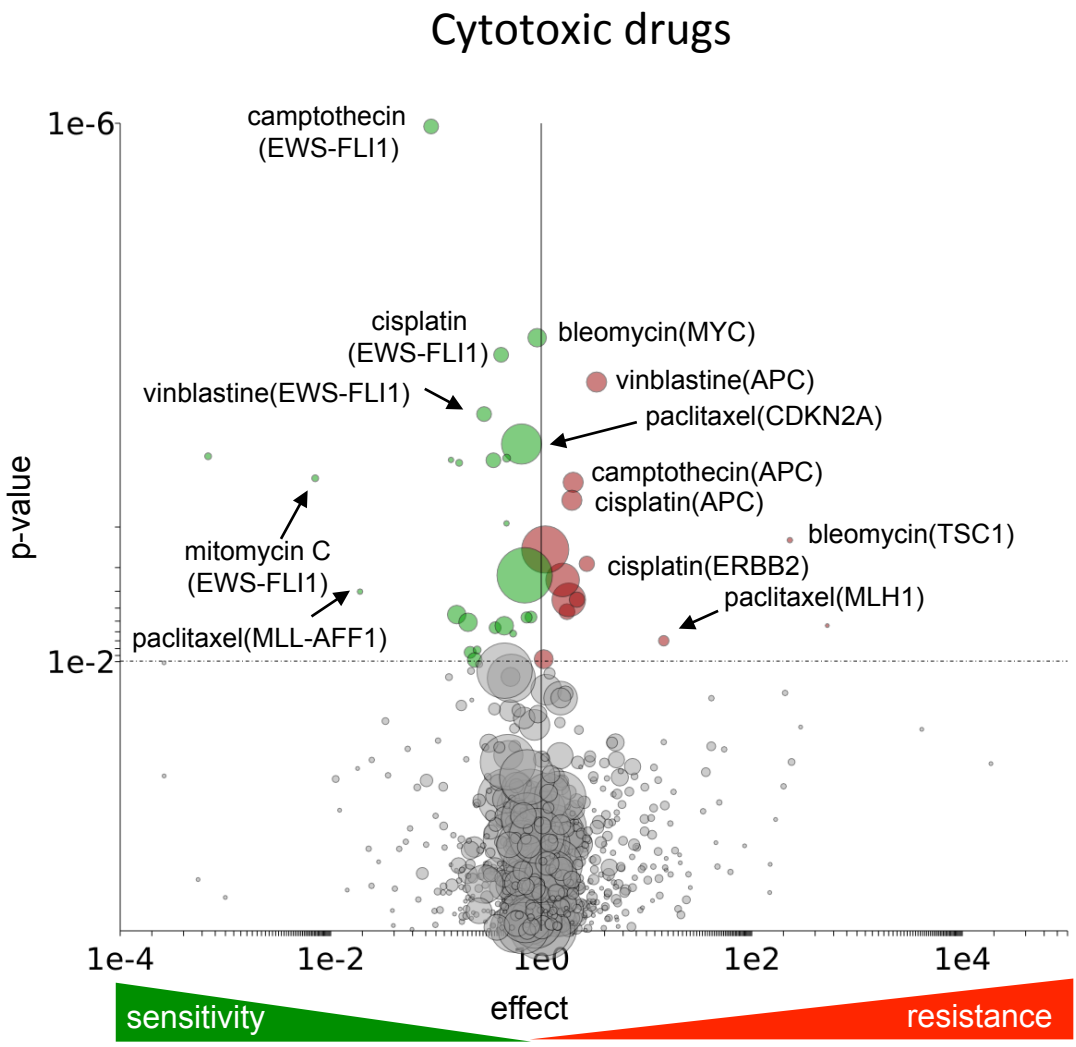

Supplementary Figure 9: Genomic markers of sensitivity to cytotoxic chemotherapeutics. A volcano plot representation of cytotoxic drugs (*n* =13 drugs) from the MANOVA showing the magnitude (effect; x-axis) and significance (p-value; inverted y-axis) of all drug-gene associations. Each circle represents a single drug-gene interaction and the circle size is proportional to the number of mutant cell lines screened (maximum = 312). The horizontal dashed line indicates the threshold of statistical significance (0.2 FDR, $P < 0.0099$) and significant associations with drug sensitivity or resistance are coloured green and red, respectively. Select significant drug-gene associations are labeled with drug name and gene name (bracketed).

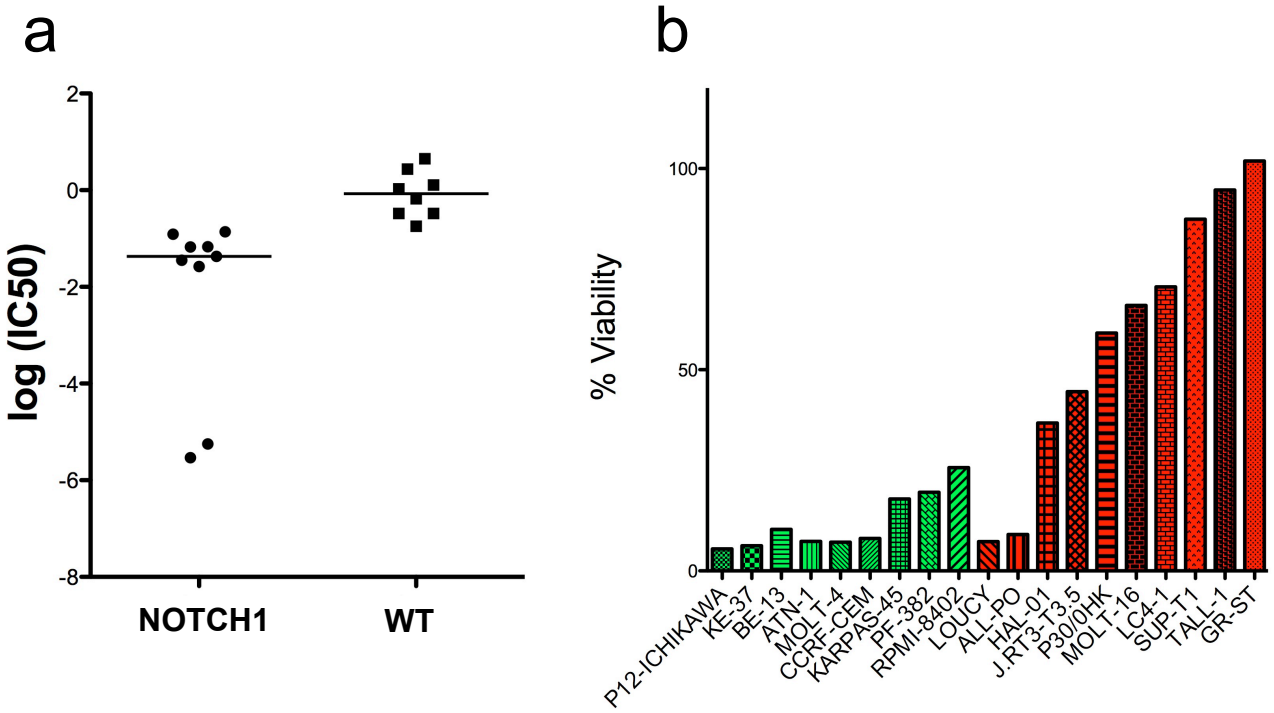

Supplementary Figure 10: Sensitivity of *NOTCH1* mutant leukemic cell lines to ABT-263 following 7 day drug treatment. A panel of leukemic lines (9 *NOTCH1* mutant and 8 wild-type) were treated for 7 days with increasing concentrations of ABT-263 (40 nM – 10 uM). **a,** The concentration of ABT-263 necessary to obtain 50% reduction in cell number (IC_{50}) was determined to be significantly lower for *NOTCH1* mutant lines ($P < 0.0001$, student t-test) than wild-type (WT) lines. **b**, Normalised cell viability following 7 days of treatment with 0.31 uM ABT-263 for *NOTCH1* mutant (green fill, n =9) and wild-type (red fill, n =10) cell lines.

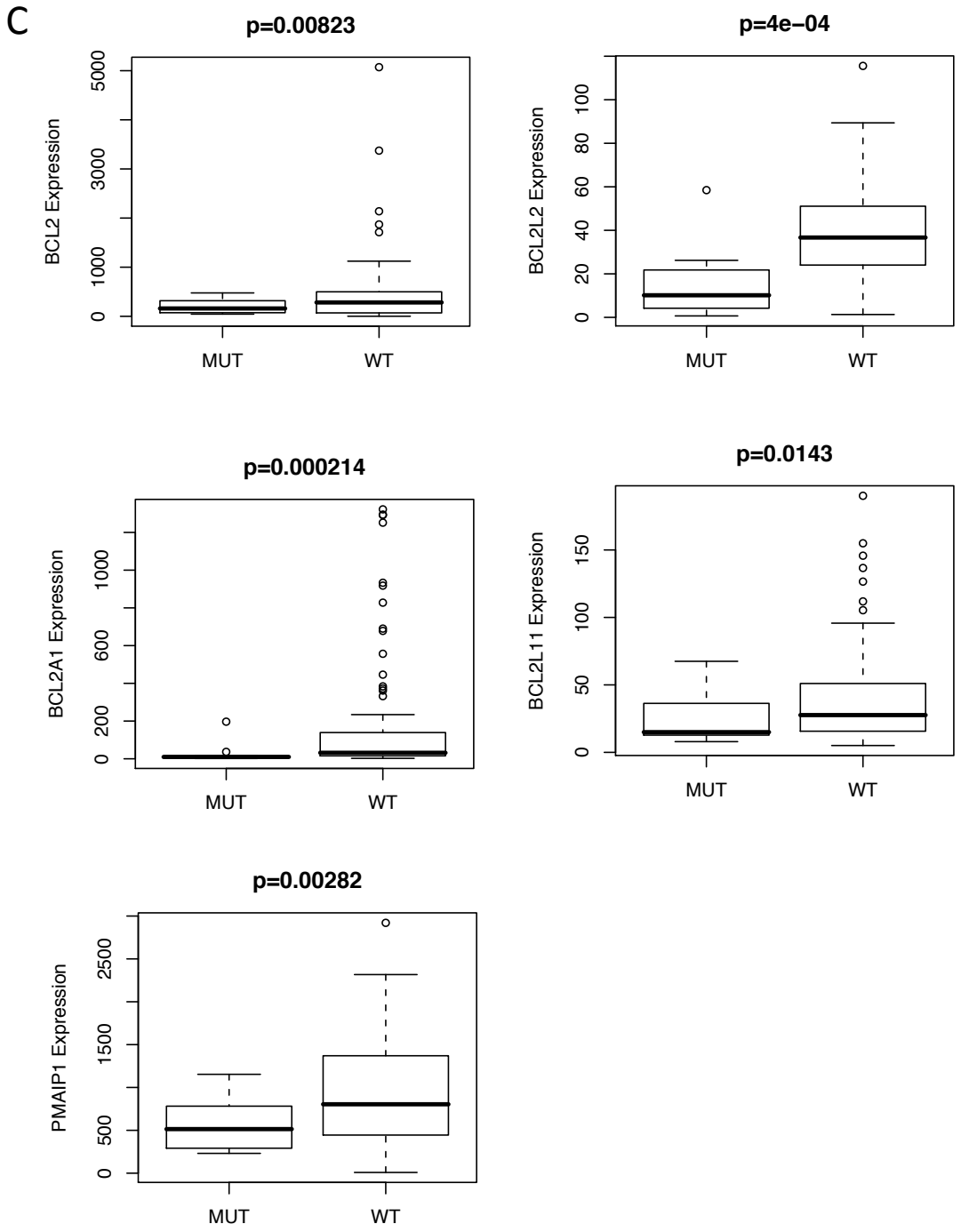

Supplementary Figure 11: **Decreased expression of apoptotic genes in *NOTCH1* mutant compared to wild-type hematopoietic cell.** Expression levels of the indicated genes were obtained from the U133A microarray dataset and statistical significance tested using student t-test. *NOTCH1* is frequently mutated in hematopoietic cell lines and so only cell lines of hematopoietic origin were considered to minimize tissue specific effects on expression (*NOTCH1* (MUT), *n* =12; wild-type (WT), *n* = 80). Additional apoptotic regulators tested were not differentially expressed (*BAD, BBC3, BCL2L10, BID, BIK, BNIP1, BNIP2, BNIP3, MCL1*).

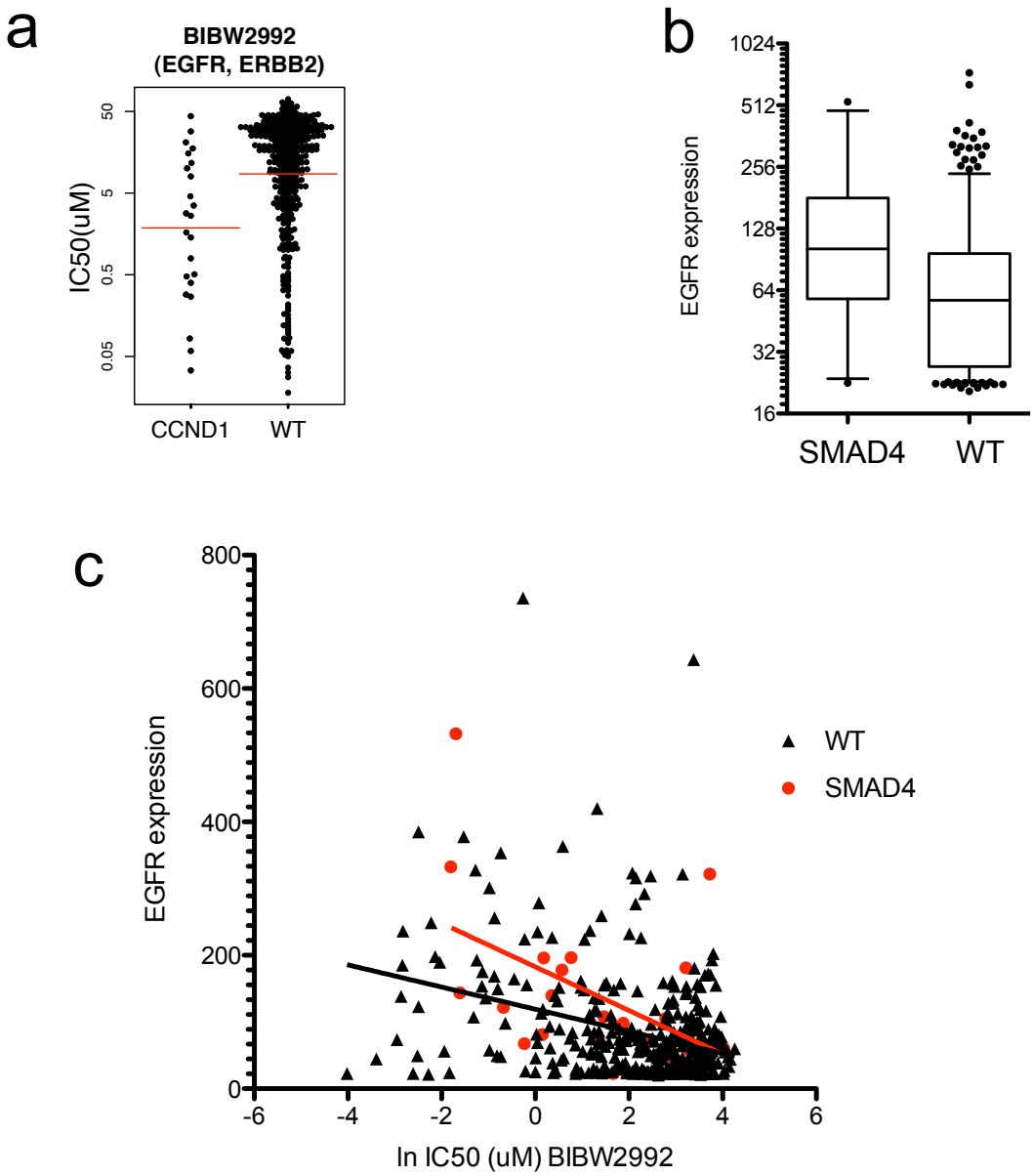

Supplementary Figure 12: Sensitivity of *SMAD4* mutated cell lines to EGFR inhibitors is associated with increased *EGFR* expression. a, A scatter plot of *CCND1* mutated or wild-type (WT) cell line IC_{50} values for BIBW29922 (P = 6.7 x10^{-4} from the MANOVA). Each circle represents the IC_{50} of one cell line on a log scale and the red line is the geometric mean. **b**, *EGFR* gene expression is elevated in *SMAD4* mutated cell lines (P = 0.0031, students t-test). A box and whisker plots of gene expression levels in wild-type (WT, n = 399) cell lines or cell lines with a *SMAD4* mutation (n = 24) . Whiskers indicate the 5th and 95th percentiles and outlier cell lines are indicated by black dots. Cell lines with *CCND1* mutation were also correlated with sensitivity to EGFR inhibitors from the MANOVA analysis but where not associated with altered *EGFR* gene expression. **c**, Cell line sensitivity to EGFR/ERBB2 inhibitor BIBW2992 is correlated with *EGFR* expression levels in WT (spearman correlation, r= -0.2051, P < 0.0001, n = 399) and *SMAD4* mutated (r= -0.5313, P = 0.0075, n = 24) cell lines. Linear regressions for WT (black line) and *SMAD4* mutated (red line) cell lines are shown. For the analysis in **b** and **c** all *EGFR* or *ERBB2* mutated cell lines were excluded.

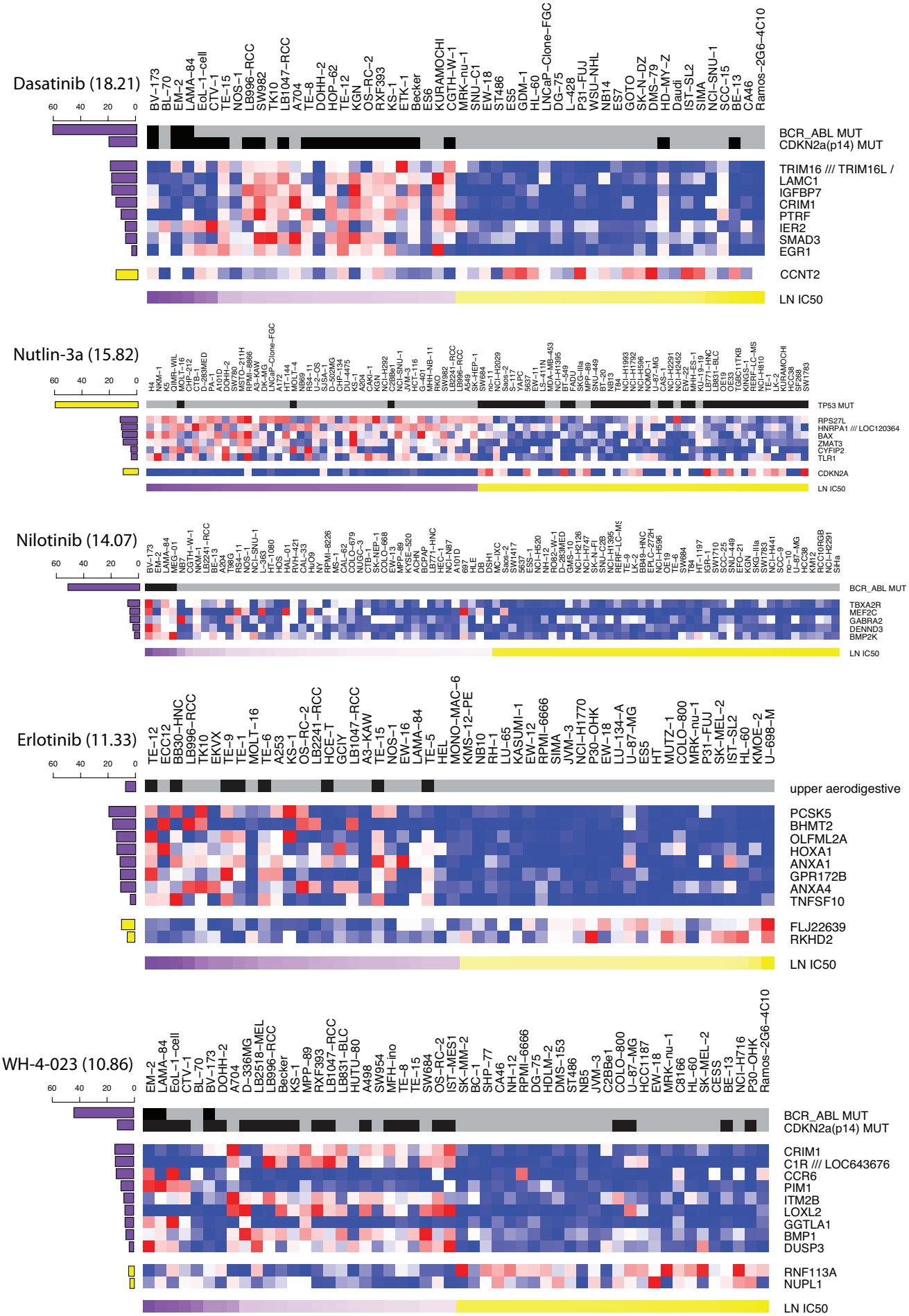
Dasatinib (18.21)
BCR_ABL MUT
CDKN2a(p14) MUT
TRIM16 /// TRIM16L /
LAMC1
IGFBP7
CRIM1
PTRF
IER2
SMAD3
EGR1
CCNT2
LN IC50
Nutlin-3a (15.82)
TP53 MUT
RPS27L
HNRPA1 /// LOC120364
BAX
ZMAT3
CYFIP2
TLR1
CDKN2A
LN IC50
Nilotinib (14.07)
BCR_ABL MUT
TBXA2R
MEF2C
GABRA2
DENND3
BMP2K
LN IC50
Erlotinib (11.33)
upper aerodigestive
PCSK5
BHMT2
OLFML2A
HOXA1
ANXA1
GPR172B
ANXA4
TNFSF10
FLJ22639
RKHD2
LN IC50
WH-4-023 (10.86)
BCR_ABL MUT
CDKN2a(p14) MUT
CRIM1
C1R /// LOC643676
CCR6
PIM1
ITM2B
LOXL2
GGTLA1
BMP1
DUSP3
RNF113A
NUPL1
LN IC50

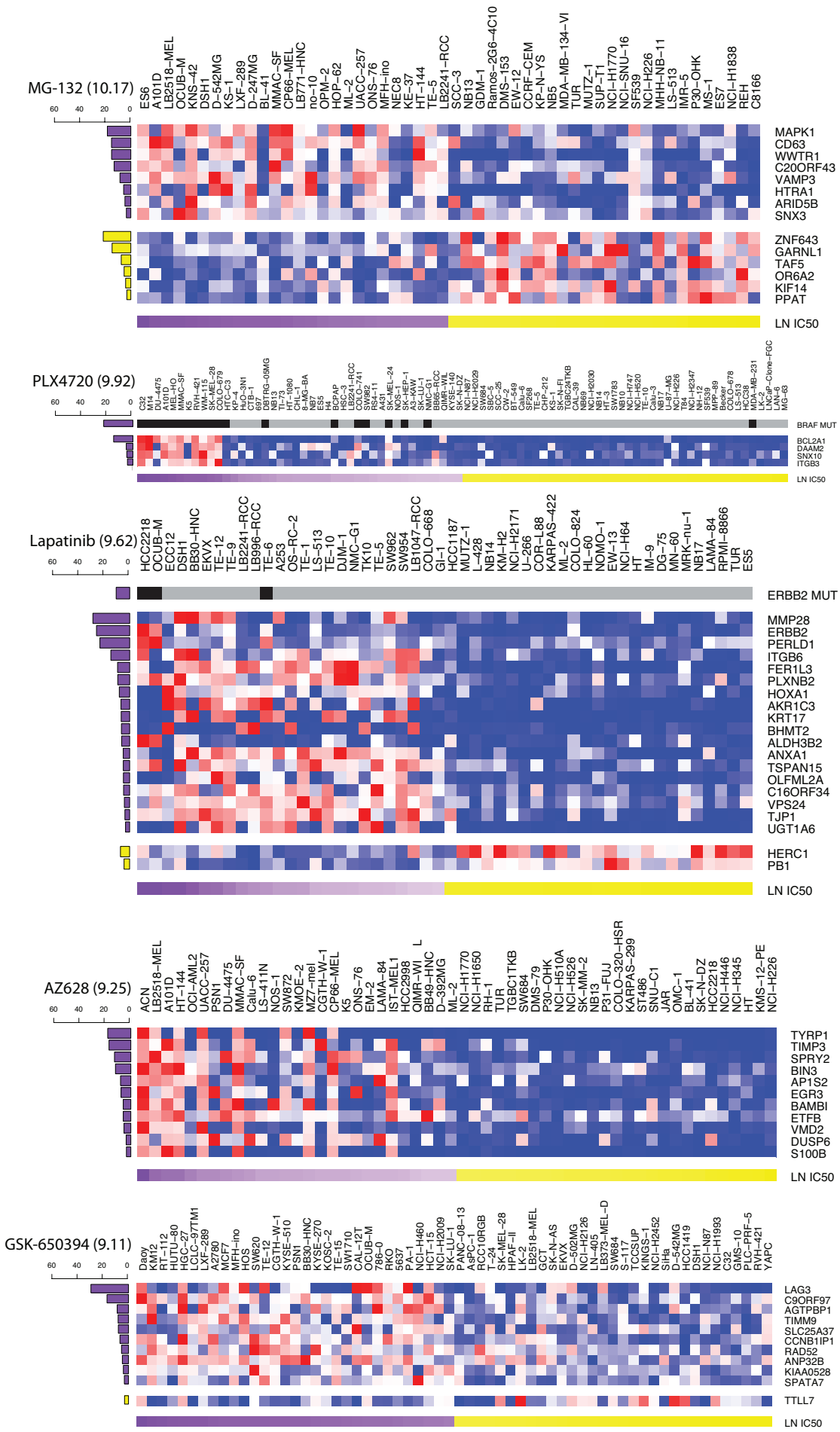
MG-132 (10.17)
60 40 20 0
ES6 A101D LB2518–MEL OCUB–M KNS–42 DSH1 D–542MG KS–1 LXF–289 D–247MG BL–41 MMAC–SF CP66–MEL LB771–HNC no–10 OPM–2 HOP–62 ML–2 UACC–257 ONS–76 MFH–ino NEC8 KE–37 HT–144 TE–5 LB2241–RCC SCC–3 NB13 GDM–1 Ramos–2G6–4C10 DMS–153 EW–12 CCRF–CEM KP–N–YS NB5 MDA–MB–134–VI TUR MUTZ–1 SUP–T1 NCI–H1770 NCI–SNU–16 SF539 NCI–H226 MHH–NB–11 LS–513 IMR–5 P30–OHK MS–1 ES7 NCI–H1838 REH C8166
MAPK1
CD63
WWTR1
C20ORF43
VAMP3
HTRA1
ARID5B
SNX3
ZNF643
GARNL1
TAF5
OR6A2
KIF14
PPAT
LN IC50
PLX4720 (9.92)
60 40 20 0
C32 G361 SK–MEL–28 DU–4475 A101D MEL–HO MMAC–SF K5 RVH–421 SW–1417 COLO–679 HTC–C3 HT–144 KIJK–3N1 CTB–1 697 NCI–H1770 NB13 TI–73 HT–1080 HT–29 8–MG–BA NB7 ES5 ES6 BCPAP HSC–3 KYSE–270 COLO–741 SW982 RS4–11 A549 SK–MEL–24 NOS–1 SK–HEP–1 A375–MAY SK–LU–1 NMC–G1 DBB–RCC TE–10 KYSE–140 SK–N–DZ NCI–H522 NCI–H2029 SW684 SBC–5 SCC–25 CW–2 BT–549 Calu–6 SW–13 TE–5 CHP–212 SK–N–FI TGBC24TKB CAL–39 KMS–11 NCIH–H2030 NB14 HT–3 SW1783 NB10 NCI–H747 NCI–H520 TE–11 Calu–3 NB17 LB–41 NCI–H226 T84 NCI–H2347 SW–1990 SF539 MPP–89 Becker TOV–21G LS–513 HCC38 MDA–MB–231 LNCaP–Clone–FGC LAN–6 MG–63
BRAF MUT
BCL2A1
DAAM2
SNX10
ITGB3
LN IC50
Lapatinib (9.62)
60 40 20 0
HCC2218 OCUB–M ECC12 DSH1 BB30–HNC EKVX TE–12 TE–9 LB2241–RCC LB996–RCC TE–6 A253 OS–RC–2 TE–1 LS–513 TE–10 DJM–1 NMC–G1 TK10 TE–5 SW962 SW954 LB1047–RCC COLO–668 GI–1 HCC1187 MUTZ–1 L–428 NB14 KM–H2 NCI–H2171 U–266 COR–L88 KARPAS–422 ML–2 COLO–824 HL–60 NOMO–1 EW–13 NCI–H64 HT IM–9 DG–75 MN–60 MRK–nu–1 NB17 LAMA–84 RPMI–8866 TUR ES5
ERBB2 MUT
MMP28
ERBB2
PERLD1
ITGB6
FER1L3
PLXNB2
HOXA1
AKR1C3
KRT17
BHMT2
ALDH3B2
ANXA1
TSPAN15
OLFML2A
C16ORF34
VPS24
TJP1
UGT1A6
HERC1
PB1
LN IC50
AZ628 (9.25)
60 40 20 0
ACN LB2518–MEL A101D HT–144 OCI–AML2 UACC–257 PSN1 DU–4475 MMAC–SF Calu–6 LS–411N NOS–1 SW872 KMOE–2 MZ7–mel CGTH–W–1 CP66–MEL K5 ONS–76 EM–2 LAMA–84 IST–MEL1 HCC2998 QIMR–WI L BB49–HNC D–392MG ML–2 NCI–H1770 NCI–H1650 RH–1 TUR TGBC1TKB SW684 DMS–79 P30–OHK NCI–H510A NCI–H526 SK–MM–2 NB13 P31–FUJ COLO–320–HSR KARPAS–299 ST486 SNU–C1 JAR OMC–1 BL–41 SK–N–DZ HCC2218 NCI–H446 NCI–H345 HT KMS–12–PE NCI–H226
TYRP1
TIMP3
SPRY2
BIN3
AP1S2
EGR3
BAMBI
ETFB
VMD2
DUSP6
S100B
LN IC50
GSK-650394 (9.11)
60 40 20 0
Daoy KM12 RT–112 HUTU–80 HGC–27 LCLC–97TM1 LXF–289 A2780 MCF7 MFH–ino SW620 TE–12 CGTH–W–1 KYSE–510 PSN1 BB30–HNC KYSE–270 KOSC–2 TE–15 TE–15 SW1710 CAL–12T OCUB–M 786–0 RKO 5637 PA–1 NCI–H460 HCT–15 NCI–H2009 SK–LU–1 PANC–08–13 AsPC–1 RCC10RGB T–24 SK–MEL–28 HPAF–II LK–2 LB2518–MEL GCT SK–N–AS EKVX D–502MG NCI–H2126 LN–405 LB373–MEL–D SW684 TCCSUP KINGS–1 NCI–H2452 SIHa D–542MG HCC1419 DSH1 NCI–N87 NCI–H1993 C32 GMS–10 PLC–PRF–5 RVH–421 YAPC
LAG3
C9ORF97
AGTPBP1
TIMM9
SLC25A37
CCNB1IP1
RAD52
ANP32B
KIAA0528
SPATA7
TTLL7
LN IC50

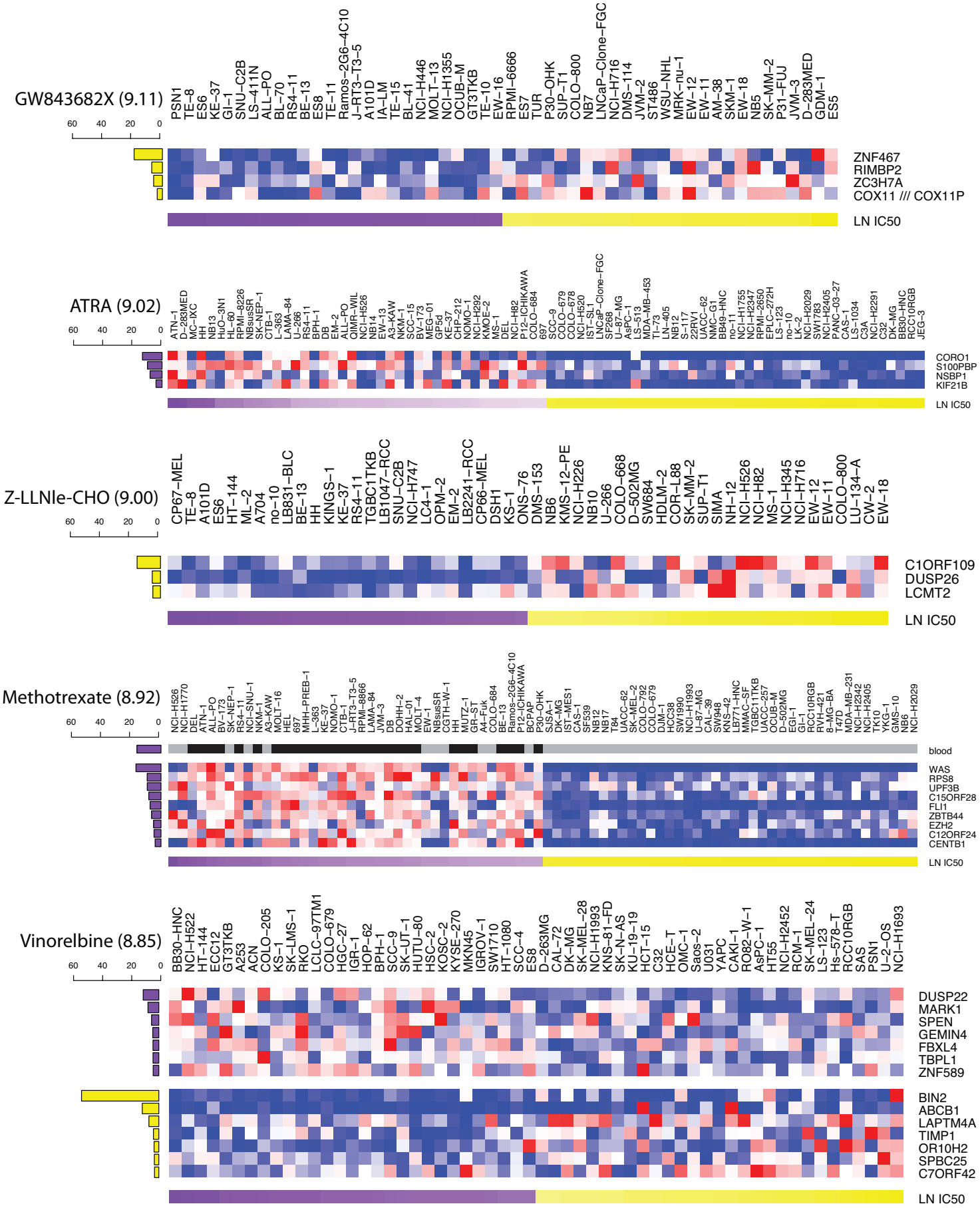
GW843682X (9.11)
60 40 20 0
PSN1 TE-8 ES6 KE-37 GI-1 SNU-C2B LS-411N ALL-PO BL-70 RS4-11 BE-13 ES8 TE-11 Ramos-2G6-4C10 J-RT3-T3-5 A101D IA-LM TE-15 BL-41 NCI-H446 MOLT-13 NCI-H1355 OCUB-M GT3TKB TE-10 EW-16 RPMI-6666 ES7 TUR P30-OHK SUP-T1 COLO-800 NB7 LNCaP-Clone-FGC NCI-H716 DMS-114 JVM-2 ST486 WSU-NHL MRK-nu-1 EW-12 EW-11 AM-38 SKM-1 EW-18 NB5 SK-MM-2 P31-FUJ JVM-3 D-283MED GDM-1 ES5
ZNF467
RIMBP2
ZC3H7A
COX11 /// COX11P
LN IC50
ATRA (9.02)
60 40 20 0
ATN-1 D-283MED MC-IXC HH NB13 HuO-3N1 HL-60 RPMI-8226 NBsusSR SK-NEP-1 CTB-1 L-363 LAMA-84 U-266 RS4-11 BPH-1 DB EM-2 ALL-PO QIMR-WIL NCI-H526 NB14 EW-13 A3-KAW NKM-1 SCC-15 BV-173 MEG-01 GP5d KE-37 CHP-212 NOMO-1 NCI-H292 KMOE-2 MS-1 DEL NCI-H82 P12-ICHIKAWA COLO-684 697 SCC-9 COLO-679 COLO-678 NCI-H520 IST-SL1 LNCaP-Clone-FGC SP268 U-87-MG AsPC-1 LS-513 MDA-MB-453 TI-73 LN-405 NB12 S-117 22RV1 UACC-62 NMC-G1 BB49-HNC no-11 NCI-H1755 NCI-H2347 RPMI-2650 EPLC-272H LS-123 no-10 LK-2 NCI-H2029 SW1783 NCI-H2405 PANC-03-27 CAS-1 LS-1034 C3A NCI-H2291 C32 DK-MG BB30-HNC RCC10RGB JEG-3
CORO1
S100PBP
NSBP1
KIF21B
LN IC50
Z-LLNle-CHO (9.00)
60 40 20 0
CP67-MEL TE-8 A101D ES6 HT-144 ML-2 A704 no-10 LB831-BLC BE-13 HH KINGS-1 KE-37 RS4-11 TGBC1TKB LB1047-RCC SNU-C2B NCI-H747 LC4-1 OPM-2 EM-2 LB2241-RCC CP66-MEL DSH1 KS-1 ONS-76 DMS-153 NB6 KMS-12-PE NCI-H226 NB10 U-266 COLO-668 D-502MG SW684 HDLM-2 COR-L88 SK-MM-2 SUP-T1 SIMA NH-12 NCI-H526 NCI-H82 MS-1 NCI-H345 NCI-H716 EW-12 EW-11 COLO-800 LU-134-A CW-2 EW-18
C1ORF109
DUSP26
LCMT2
LN IC50
Methotrexate (8.92)
60 40 20 0
NCI-H526 NCI-H1770 DEL ATN-1 ALL-PO BV-173 SK-NEP-1 RS4-11 NCI-SNU-1 NKM-1 A3-KAW MOLT-16 HEL 697 MHH-PREB-1 L-363 KE-37 NOMO-1 CTB-1 J-RT3-T3-5 RPMI-8866 LAMA-84 JVM-3 DB DOHH-2 HAL-01 MOLT-4 EW-1 NBsusSR CGTH-W-1 HH MUTZ-1 GR-ST A4-Fuk COLO-684 BE-13 Ramos-2G6-4C10 P12-ICHIKAWA BCPAP P30-OHK SJSA-1 DK-MG IST-MES1 CAS-1 SF539 NB12 NB17 T84 UACC-62 SK-MEL-2 COLO-792 COLO-679 DJM-1 HCC38 SW1990 NCI-H1993 U-87-MG CAL-39 SW948 KNS-42 LB771-HNC MMAC-SF TGBC11TKB UACC-257 OCUB-M D-502MG EGI-1 GI-1 RCC10RGB RVH-421 8-MG-BA T47D MDA-MB-231 NCI-H2342 NCI-H2405 TK10 YKG-1 GMS-10 NB6 NCI-H2029
blood
WAS
RPS8
UPF3B
C15ORF28
FLI1
ZBTB44
EZH2
C12ORF24
CENTB1
LN IC50
Vinorelbine (8.85)
60 40 20 0
BB30-HNC NCI-H522 HT-144 ECC12 GT3TKB A253 ACN COLO-205 KS-1 SK-LMS-1 RKO LCLC-97TM1 COLO-679 HGC-27 IGR-1 HOP-62 BPH-1 SCC-9 SK-UT-1 HUTU-80 HSC-2 KOSC-2 KYSE-270 MKN45 IGROV-1 SW1710 HT-1080 SCC-4 ES8 D-263MG CAL-72 DK-MG SK-MEL-28 NCI-H1993 KNS-81-FD SK-N-AS KU-19-19 HCT-15 C32 HCE-T OMC-1 Saos-2 U031 YAPC CAKI-1 RO82-W-1 AsPC-1 HT55 NCI-H2452 RCM-1 SK-MEL-24 LS-123 Hs-578-T RCC10RGB SAS PSN1 U-2-OS NCI-H1693
DUSP22
MARK1
SPEN
GEMIN4
FBXL4
TBPL1
ZNF589
BIN2
ABCB1
LAPTM4A
TIMP1
OR10H2
SPBC25
C7ORF42
LN IC50

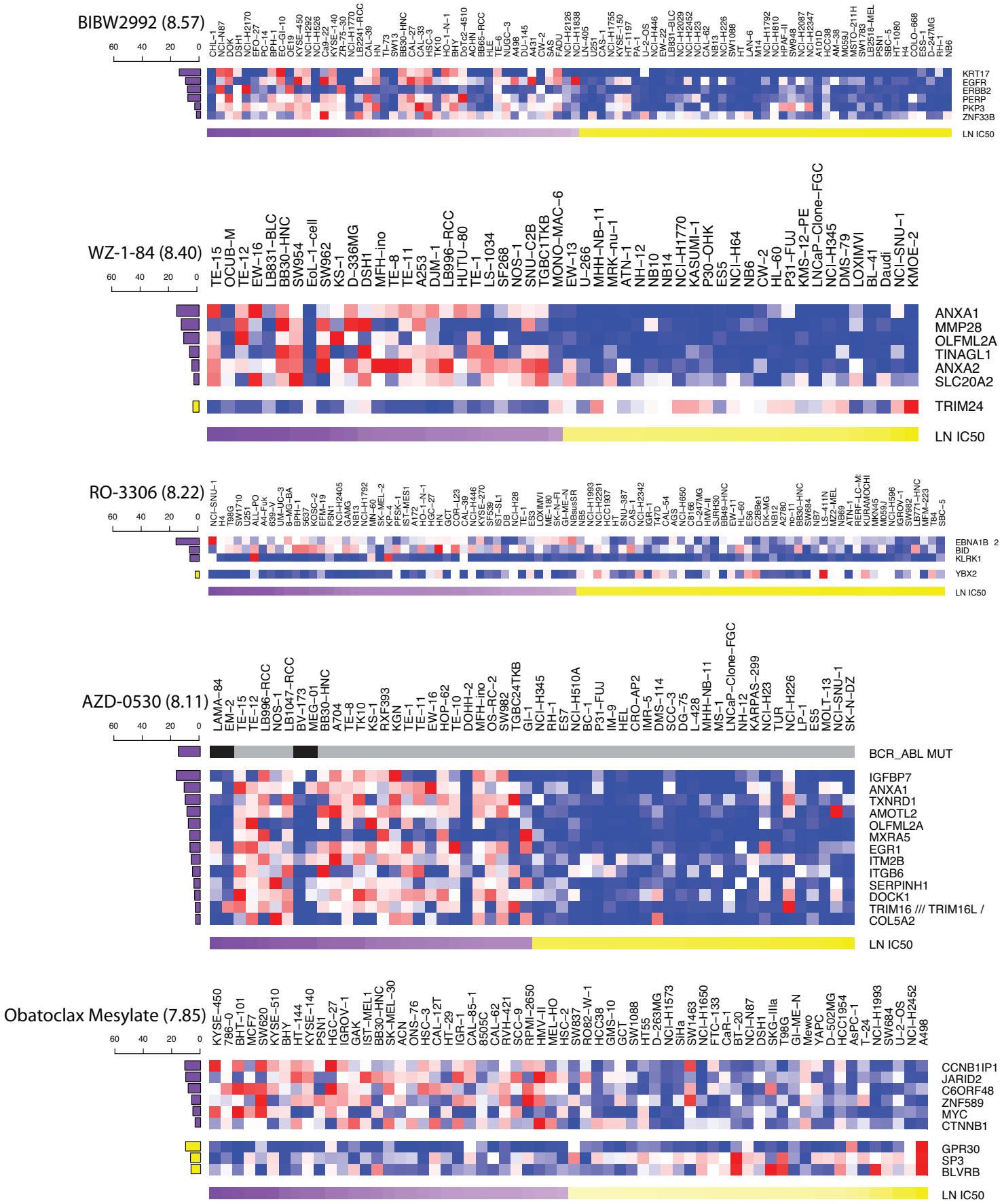
BIBW2992 (8.57)
60 40 20 0
CHL−1 NCI−N87 DOK DSH1 NCI−H2170 EFO−27 PC−14 BPH−1 EC−GI−10 KYSE−450 NCI−H292 NCI−H526 Ca9−22 KYSE−140 ZR−75−30 NCI−H1770 LB2241−RCC CAL−39 HN TT−3 SW13 BB30−HNC CAL−27 CAL−33 HSC−3 TK10 HO−1−N−1 BHY DoTc2−4510 ACHN BB65−RCC HLE TE−6 NUGC−3 A498 DU−145 A431 CW−2 SAS FADU NCI−H2126 NCI−H838 NCI−H405 U251 CAS−1 NCI−H1755 KYSE−150 HT−1197 PA−1 U−2−OS NCI−H446 EW−22 LB831−BLC NCI−H2029 NCI−H2052 NCI−H23 CAL−62 NB13 NCI−H226 SW1088 HT LAN−6 M14 NCI−H1792 NCI−H810 HPAF−II SW948 NCI−H2087 NCI−H2347 A101D HCC38 AM−38 M059J MSTO−211H SW1783 LB2518−MEL RPMI−1 SBC−5 HT−1080 H4 COLO−668 ESS−1 D−247MG RH−1 NB6
KRT17
EGFR
ERBB2
PERP
PKP3
ZNF33B
LN IC50
WZ−1−84 (8.40)
60 40 20 0
TE−15 OCUB−M TE−12 EW−16 LB831−BLC BB30−HNC SW954 EoL−1−cell SW962 KS−1 D−336MG DSH1 MFH−ino TE−8 TE−11 A253 DJM−1 LB996−RCC HUTU−80 TE−1 LS−1034 SF268 NOS−1 SNU−C2B TGBC1TKB MONO−MAC−6 EW−13 U−266 MHH−NB−11 MRK−nu−1 ATN−1 NH−12 NB10 NB14 NCI−H1770 KASUMI−1 P30−OHK ES5 NCI−H64 NB6 CW−2 HL−60 P31−FUJ KMS−12−PE LNCaP−Clone−FGC NCI−H345 DMS−79 LOXIMVI BL−41 Daudi NCI−SNU−1 KMOE−2
ANXA1
MMP28
OLFML2A
TINAGL1
ANXA2
SLC20A2
TRIM24
LN IC50
RO−3306 (8.22)
60 40 20 0
NCI−SNU−1 H4 T98G SW1710 U251 ALL−PO A4−Fuk G39−LC−3 8−MG−BA BPH−1 5637 KOSC−2 EFM−19 PSN1 NCI−H2405 BAY3 NCI−H1792 MN−60 SK−MEL−2 KP−4 PFSK−1 IST−MES1 A172 HAL−1−N−1 HGC−27 HN GCT COR−L23 CAL−39 NCI−H446 KYSE−270 IST−EW1 IST−SL1 DB NCI−H28 TE−1 ES3 LOXIMVI ME−180 SK−ME−1 SK−ME−5 NBsusSR NB5 NCI−H1993 NCI−H2291 HCC1937 HT SNU−387 CS−1 NCI−H2342 IGR−1 T47D CAL−54 AGS NCI−H650 C8166 D−247MG HMC−1−8 SJRH30 BB49−HNC EW−11 HL−60 ES6 C2BBe1 NK−MG NB−17 A2780 no−11 BB30−HNC SW684 NB7 LS−411N NZ2−MEL NB69 ATN−1 RERF−LC−MS KURAMOCHI MKN45 M059J NCI−H596 IGROV−1 SW982 SW872−HNC MFM−223 TB4 SBC−5
EBNA1B 2
BID
KLRK1
YBX2
LN IC50
AZD−0530 (8.11)
60 40 20 0
LAMA−84 EM−2 TE−15 TE−12 LB996−RCC NOS−1 LB1047−RCC BV−173 MEG−01 BB30−HNC A704 TE−8 TK10 KS−1 RXF393 KGN TE−1 TE−11 EW−16 HOP−62 TE−10 DOHH−2 MFH−ino OS−RC−2 SW982 TGBC24TKB GI−1 NCI−H345 RH−1 ES7 NCI−H510A BC−1 P31−FUJ IM−9 HEL CRO−AP2 IMR−5 DMS−114 SCC−3 DG−75 L−428 MHH−NB−11 MS−1 LNCaP−Clone−FGC NH−12 KARPAS−299 NCI−H23 TUR NCI−H226 LP−1 ES5 MOLT−13 NCI−SNU−1 SK−N−DZ
BCR_ABL MUT
IGFBP7
ANXA1
TXNRD1
AMOTL2
OLFML2A
MXRA5
EGR1
ITM2B
ITGB6
SERPINH1
DOCK1
TRIM16 /// TRIM16L /
COL5A2
LN IC50
Obatoclax Mesylate (7.85)
60 40 20 0
KYSE−450 786−0 BHT−101 MCF7 SW620 KYSE−510 BHY HT−144 KYSE−140 PSN1 HGC−27 IGROV−1 GAK IST−MEL1 BB30−HNC SK−MEL−30 ACN ONS−76 HSC−3 CAL−12T HT−29 IGR−1 CAL−85−1 8505C CAL−62 RVH−421 SCC−9 RPMI−2650 HMV−II MEL−HO HSC−2 SW837 RO82−W−1 HCC38 GMS−10 GCT SW1088 HT55 D−263MG NCI−H1573 SIHa SW1463 NCI−H1650 FTC−133 CaR−1 BT−20 NCI−N87 DSH1 SKG−IIIa T98G GI−ME−N Mewo YAPC D−502MG HCC1954 AsPC−1 T−24 NCI−H1993 SW684 U−2−OS NCI−H2452 A498
CCNB1IP1
JARID2
C6ORF48
ZNF589
MYC
CTNNB1
GPR30
SP3
BLVRB
LN IC50

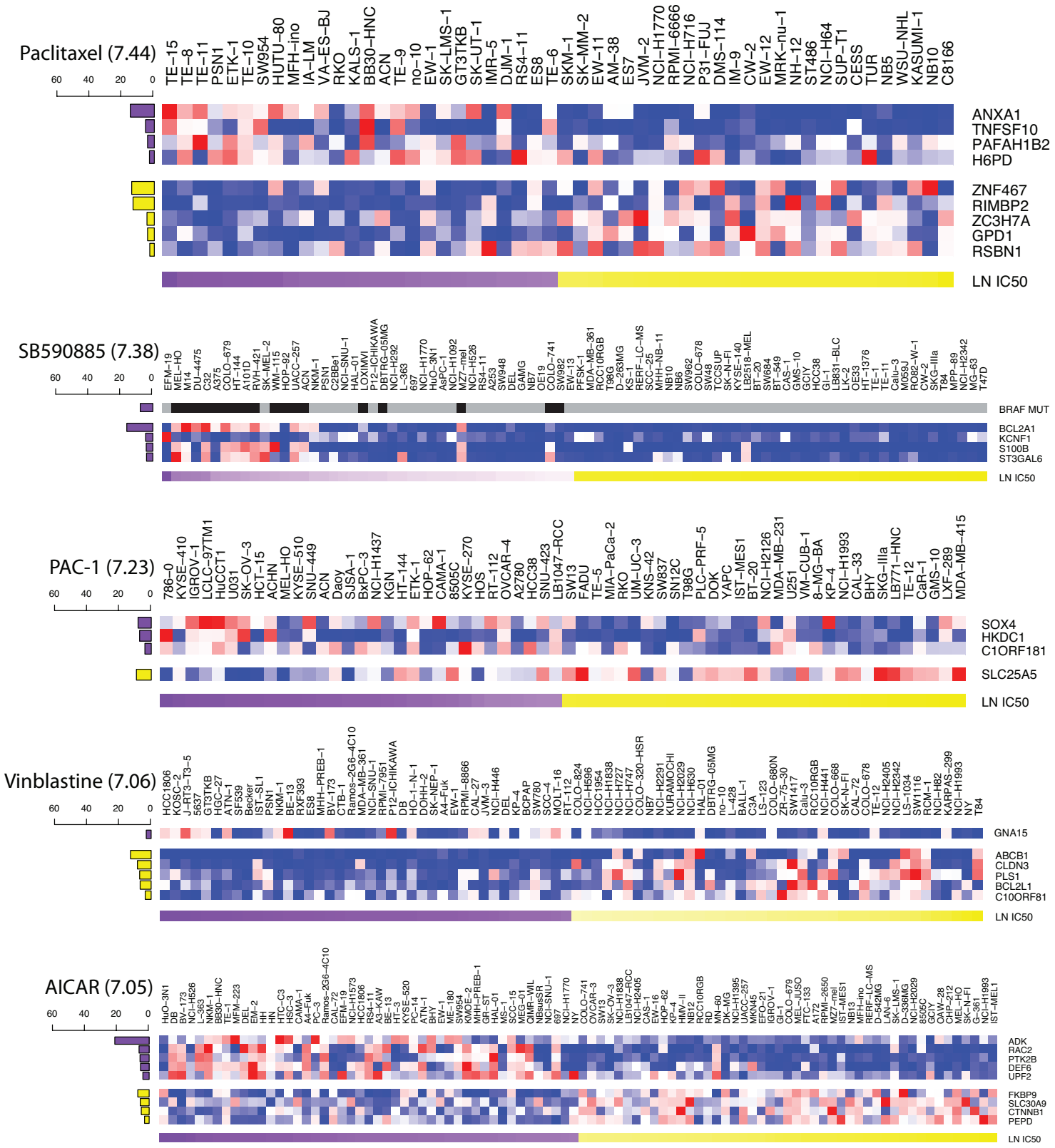
Paclitaxel (7.44)
60 40 20 0
TE–15 TE–8 TE–11 PSN1 ETK–1 TE–10 SW954 HUTU–80 MFH–ino IA–LM VA–ES–BJ RKO KALS–1 BB30–HNC ACN TE–9 no–10 EW–1 SK–LMS–1 GT3TKB SK–UT–1 IMR–5 DJM–1 RS4–11 ES8 TE–6 SKM–1 SK–MM–2 EW–11 AM–38 ES7 JVM–2 NCI–H1770 RPMI–6666 NCI–H716 P31–FUJ DMS–114 IM–9 CW–2 EW–12 MRK–nu–1 NH–12 ST486 NCI–H64 SUP–T1 CESS TUR NB5 WSU–NHL KASUMI–1 NB10 C8166
ANXA1
TNFSF10
PAFAH1B2
H6PD
ZNF467
RIMBP2
ZC3H7A
GPD1
RSBN1
LN IC50
SB590885 (7.38)
60 40 20 0
EFM–19 MEL–HO M14 DU–4475 C32 A375 COLO–679 HT–144 A101D RVH–421 SK–MEL–2 WM–115 HOP–92 IACC–257 ACN NKM–1 PSBe1 CAL–51 SNU–1 HAL–01 LOXIMVI P12–ICHIKAWA DBTRG–05MG NCI–H292 L–363 697 NCI–H1770 HuO–3N1 AsPC–1 NCI–H1092 MZ7–mel NCI–H526 RS4–11 A253 SW948 DEL GAMG NB7 OE19 COLO–741 SW982 EW–13 PFSK–1 MDA–MB–361 RCC10RGB T98G D–283MG KS–1 RERF–LC–MS SCC–25 MHH–NB–11 NB10 NB6 SW962 COLO–678 SW48 TCCSUP SK–N–FI KYSE–140 LB2518–MEL BT–20 SW684 BT–549 CAS–1 GMS–10 GCIY HCC38 GI–1 LB831–BLC LK–2 OE33 HT–1376 TE–1 TE–11 Calu–3 M059J RD82–W–1 CWR–2 SKG–IIIa TB1 MPP–89 NCI–H2342 MG–63 T47D
BRAF MUT
BCL2A1
KCNF1
S100B
ST3GAL6
LN IC50
PAC–1 (7.23)
60 40 20 0
786–0 KYSE–410 IGROV–1 LCLC–97TM1 HuCCT1 U031 SK–OV–3 HCT–15 ACHN MEL–HO KYSE–510 SNU–449 ACN Daoy SJSA–1 BxPC–3 NCI–H1437 KGN HT–144 ETK–1 HOP–62 CAMA–1 8505C KYSE–270 HOS RT–112 OVCAR–4 A2780 HCC38 SNU–423 LB1047–RCC SW13 FADU TE–5 MIA–PaCa–2 RKO UM–UC–3 KNS–42 SW837 SN12C T98G PLC–PRF–5 DOK YAPC IST–MES1 BT–20 NCI–H2126 MDA–MB–231 U251 VM–CUB–1 8–MG–BA KP–4 NCI–H1993 CAL–33 BHY SKG–IIIa LB771–HNC TE–12 CaR–1 GMS–10 LXF–289 MDA–MB–415
SOX4
HKDC1
C1ORF181
SLC25A5
LN IC50
Vinblastine (7.06)
60 40 20 0
HCC1806 KOSC–2 J–RT3–T3–5 5637 GT3TKB HGC–27 ATN–1 SF539 Becker IST–SL1 PSN1 NKM–1 BE–13 RXF393 ES8 MHH–PREB–1 BV–173 CTB–1 Ramos–2G6–4C10 MDA–MB–361 NCI–SNU–1 RPMI–7951 P12–ICHIKAWA DB HO–1–N–1 DOHH–2 SK–NEP–1 A4–Fuk EW–1 RPMI–8866 CAL–27 JVM–3 NCI–H446 DEL KP–4 BCPAP SW780 SCO–4 MOLT–16 RT–112 COLO–824 NCI–H596 NCI–H1838 HCC1954 NCI–H727 NCI–H747 COLO–320–HSR NB7 NCI–H2291 KURAMOCHI NCI–H2029 NCI–H630 HAL–01 DBTRG–05MG no–10 L–428 BALL–1 C3A LS–123 COLO–680N ZR–75–30 SW1417 Calu–3 RCC10RGB NCI–H441 COLO–668 SK–N–FI CAL–72 COLO–678 TE–12 NCI–H2405 NCI–H2342 LS–1034 SW1116 RCM–1 NCI–H82 KARPAS–299 NCI–H1993 NY T84
GNA15
ABCB1
CLDN3
PLS1
BCL2L1
C10ORF81
LN IC50
AICAR (7.05)
60 40 20 0
HuO–3N1 DB BV–173 NCI–H526 L–363 NKM–1 BB30–HNC TE–1 MFM–223 DEL EW–2 HH HN HTC–C3 HSC–3 CAMA–1 A4–Fuk PC–3 Ramos–2G6–4C10 TE–8 EFM–19 NCI–H1573 HCC1806 RS4–11 A3–KAW BE–13 HT–3 KYSE–520 RC–14 ATN–1 BHY EW–1 ME–180 SW954 KMOE–2 MHH–PREB–1 GR–ST JVM–3 MG–01 SCC–15 MEG–01 QIMR–WIL NBsusSR NCI–SNU–1 697 NCI–H1770 RT–112 COLO–741 OVCAR–3 SW13 SK–OV–3 NCI–H1838 LB1047–RCC NCI–H2405 CAS–1 EW–16 EW–18 KP–4 HMV–II NB12 RCC10RGB RD MN–60 DK–MG NCI–H1395 UACC–257 MKN45 EFO–21 IGROV–1 GI–1 COLO–679 MEL–JUSO FTC–133 A172 MZM–2650 MZM–mel IST–MES1 NB13 MFH–ino RERF–LC–MS D–542MG LAN–6 SK–LMS–1 D–336MG NCI–H2029 8505C GCIY OAW–28 CHP–212 MEL–HO SK–N–FI G–361 NCI–H1993 IST–MEL1
ADK
RAC2
PTK2B
DEF6
UPF2
FKBP9
SLC30A9
CTNNB1
PEPD
LN IC50

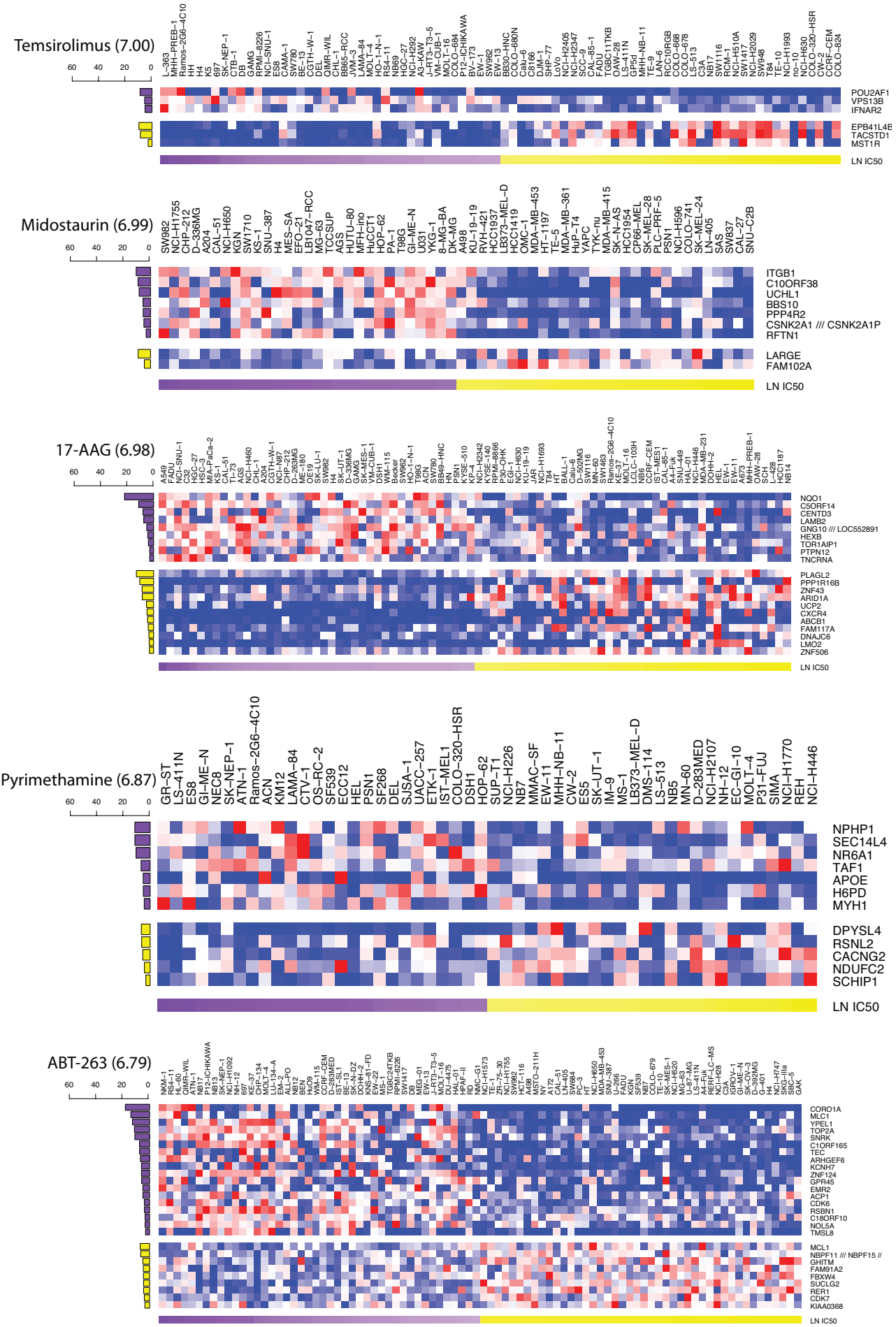
Temsirolimus (7.00)
60 40 20 0
L-363
MHH-PREB-1
Ramos-2G6-4C10
H4
K5
697
SK-NEP-1
CTB-1
DB
GAMG
RPMI-8226
ES8
SNU-1
CAMA-1
SW780
BE-13
CGTH-W-1
DEL
OMR-WIL
H1-1
BB65-RCC
JVM-3
LAMA-84
MOLT-4
HO-1-N-1
RS4-11
NB69
HCC-27
NCI-H292
A3-KAW
J-RT3-T3-5
VM-CUB-1
MOLT-16
COLO-684
TT2-CHIKAWA
BV-173
EW-1
SW962
EW-13
BB30-HNC
COLO-680N
Calu-6
ES5
DUM-1
SHP-77
LoVo
NCI-H2405
NCI-H2347
SCC-9
FADU
TGBC11TKB
OAW-28
LS-411N
GP5d
MHH-NB-11
TE-9
A4-Fuk
RC-0RGB
COLO-668
COLO-678
LS-513
C3A
NB17
SW1116
RCH-1
NCI-H510A
SW1417
NCI-H2029
SW948
TB4
TE-10
NCI-H1993
NCI-H10
NCI-H630
COLO-320-HSR
CW-2
CCRF-CEM
COLO-824
POU2AF1
VPS13B
IFNAR2
EPB41L4B
TACSTD1
MST1R
LN IC50
Midostaurin (6.99)
60 40 20 0
SW982
NCI-H1755
CHP-212
D-336MG
A204
CAL-51
NCI-H650
KGN
SW1710
KS-1
SNU-387
H4
MES-SA
EFO-21
LB1047-RCC
MG-63
TCCSUP
AGS
HUTU-80
MFH-ino
HuCCT1
HOP-62
PA-1
T98G
GI-ME-N
U031
YKG-1
8-MG-BA
DK-MG
A498
KU-19-19
RVH-421
HCC1937
LB373-MEL-D
HCC14419
OMC-1
MDA-MB-453
HT-1197
TE-5
MDA-MB-361
HuP-T4
YAPC
TYK-nu
MDA-MB-415
SK-N-AS
HCC1954
CP66-MEL
SK-MEL-28
PLC-PRF-5
PSN1
NCI-H596
COLO-741
SK-MEL-24
LN-405
SAS
SW837
CAL-27
SNU-C2B
ITGB1
C10ORF38
UCHL1
BBS10
PPP4R2
CSNK2A1 /// CSNK2A1P
RFTN1
LARGE
FAM102A
LN IC50
17-AAG (6.98)
60 40 20 0
A549
FADU
RCC-10
SNU-1
C32
HGC-27
HSC-3
MIA-PaCa-2
K5
CAL-51
TI-73
AGS
NCI-H460
CHL-1
A204
CGTH-W-1
NCI-N87
OAW-42
D-263MG
ME-180
OE19
SK-LU-1
SW982
H4
SK-UT-1
D-336MG
SK-MES-1
VM-CUB-1
DSH1
WM-115
Daudi
SW982
HO-1-N-1
T98G
A375
SW780
BB49-HNC
HN
PSN1
KYSE-510
K562
NCI-H2342
KYSE-140
RPMI-8866
ES8
SJ-GBM2
NCI-H630
KU-19-19
IAR
NCI-H1693
T84
HT
BALL-1
Calu-3
D-336MG
SW1463
Ramos-2G6-4C10
KE-37
MOLT-16
LCLC-103H
NB6
CCRF-CEM
IST-MES1
CAL-85-1
A4-Fuk
SNU-449
HAL-01
NCI-H446
MDA-MB-231
DOHH-2
ES2
EW-1
A673
MHH-PREB-1
OAW-28
SCC-9
L-428
HCC1187
NB14
NQO1
C5ORF14
CENTD3
LAMB2
GNG10 /// LOC552891
HEXB
TOR1AIP1
PTPN12
TNCRNA
PLAGL2
PPP1R16B
ZNF43
ARID1A
UCP2
CXCR4
ABCB1
FAM117A
DNAJC6
LMO2
ZNF506
LN IC50
Pyrimethamine (6.87)
60 40 20 0
GR-ST
LS-411N
ES8
GI-ME-N
NEC8
SK-NEP-1
ATN-1
Ramos-2G6-4C10
ACN
KM12
LAMA-84
CTV-1
OS-RC-2
SF539
ECC12
HEL
PSN1
SF268
DEL
SJSA-1
UACC-257
ETK-1
IST-MEL1
COLO-320-HSR
DSH1
HOP-62
SUP-T1
NCI-H226
NB7
MMAC-SF
EW-11
MHH-NB-11
CW-2
ES5
SK-UT-1
IM-9
MS-1
LB373-MEL-D
DMS-114
LS-513
NB5
MN-60
D-283MED
NCI-H2107
NH-12
EC-GI-10
MOLT-4
P31-FUJ
SIMA
NCI-H1770
REH
NCI-H446
NPHP1
SEC14L4
NR6A1
TAF1
APOE
H6PD
MYH1
DPYSL4
RSNL2
CACNG2
NDUFC2
SCHIP1
LN IC50
ABT-263 (6.79)
60 40 20 0
NKM-1
RS4-11
HL-60
OMR-WIL
ATN-1
PB1
TT2-CHIKAWA
NB13
SK-NEP-1
NCI-H1092
KS-12
697
KE-37
WM-115
MOLT-134
LU-134-A
EM-2
SK-N-DZ
NB12
BEN
HuO9
SK-N-AS
CCRF-CEM
D-283MED
IST-SL1
SK-N-SH
DOHH-2
KNS-81-FD
NB-22
MS-1
TGBC24TKB
RPMI-8226
NCI-H417
DB
MEG-01
EW-13
J-RT3-T3-5
MOLT-16
DU-4475
HAL-01
RPMI-7951
RD
NMC-G1
NCI-H1573
TE-1
ZR-75-30
NCI-H1755
SW982
HCC-70
A498
MSTO-211H
NY
A172
CAL-51
LN-405
SW684
KP-3
HT
NCI-H650
MDA-MB-453
SNU-387
U-266
FADU
KGN
NB39
NB7
COLO-679
EC-10
SK-MES-1
NCI-H520
MG-63
U-87-MG
LS-411N
A4-Fuk
RERF-LC-MS
NCI-H28
CCK-81
IGROV-1
GI-ME-N
SK-MEL-3
D-392MG
G-401
H4
NCI-H747
SKG-IIIa
SBC-5
GAK
CORO1A
MLC1
YPEL1
TOP2A
SNRK
C1ORF165
TEC
ARHGEF6
KCNH7
ZNF124
GPR45
EMR2
ACP1
CDK6
RSBN1
C18ORF10
NOL5A
TMSL8
MCL1
NBPF11 /// NBPF15 //
GHITM
FAM91A2
FBXW4
SUCLG2
RER1
CDK7
KIAA0368
LN IC50

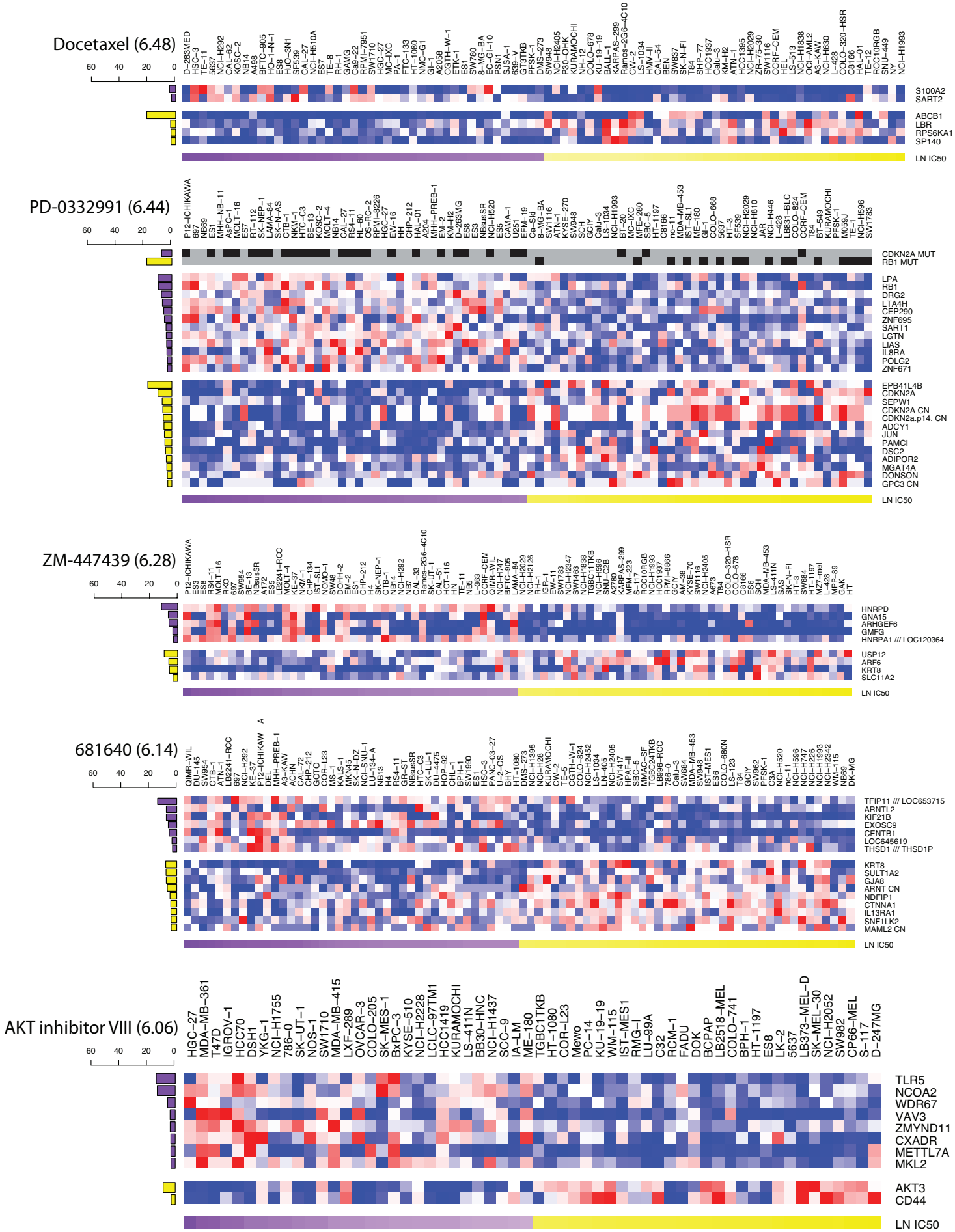
Docetaxel (6.48)
60 40 20 0
S100A2
SART2
ABCB1
LBR
RPS6KA1
SP140
LN IC50
PD-0332991 (6.44)
60 40 20 0
CDKN2A MUT
RB1 MUT
LPA
RB1
DRG2
LTA4H
CEP290
ZNF695
SART1
LGTN
LIAS
IL8RA
POLG2
ZNF671
EPB41L4B
CDKN2A
SEPW1
CDKN2A CN
CDKN2a.p14. CN
ADCY1
JUN
PAMCI
DSC2
ADIPOR2
MGAT4A
DONSON
GPC3 CN
LN IC50
ZM-447439 (6.28)
60 40 20 0
HNRPD
GNA15
ARHGEF6
GMFG
HNRPA1 /// LOC120364
USP12
ARF6
KRT8
SLC11A2
LN IC50
681640 (6.14)
60 40 20 0
TFIP11 /// LOC653715
ARNTL2
KIF21B
EXOSC9
CENTB1
LOC645619
THSD1 /// THSD1P
KRT8
SULT1A2
GJA8
ARNT CN
NDFIP1
CTNNA1
IL13RA1
SNF1LK2
MAML2 CN
LN IC50
AKT inhibitor VIII (6.06)
60 40 20 0
TLR5
NCOA2
WDR67
VAV3
ZMYND11
CXADR
METTL7A
MKL2
AKT3
CD44
LN IC50

Etoposide (5.29)
60 40 20 0
A253 EW-16 HT-144 SK-UT-1 8-MG-BA BB30-HNC ACN HGC-27 HT-1080 SW982 SW620 PA-1 ES8 COLO-679 IGROV-1 DJM-1 HUTU-80 A204 NCI-H460 MES-SA KYSE-270 SK-HEP-1 COLO-205 H4 AGS KS-1 KGN M059J Daoy KU-19-19 IST-MES1 DOK PANC-08-13 LB373-MEL-D SK-MEL-28 KNS-81-FD SK-N-AS MDA-MB-415 D-542MG HCC70 AsPC-1 U-118-MG EKVX TGBC24TKB SiHa MDA-MB-453 NCI-H1993 NCI-H2452 U-2-OS WM-115 DK-MG SW1088 S-117 C32 NCI-H727 HCC1419 D-263MG Hs-578-T
MRPS31
RNASEH2B
CCNB1IP1
ZNF202
ICAM3
DSTN
LN IC50
CEP-701 (5.27)
60 40 20 0
RPL10A
HNRPA1 /// LOC120364
EPB41L4B
TUFT1
LN IC50
BMS-536924 (5.09)
60 40 20 0
KM12 NOS-1 ETK-1 KS-1 TE-11 EW-1 TE-12 EW-16 ML-2 LB771-HNC ATN-1 TGBC24TKB L-363 MFH-ino ALL-PO PSN1 ES6 GCIY SJSA-1 HUTU-80 RS4-11 LS-411N MMAC-SF TE-8 OPM-2 NCI-H1355 Ramos-2G6-4C10 SK-MEL-2 Raji LB647-SCLC SBC-1 NB6 SK-MM-2 C8166 NCI-H1395 KE-37 NB5 IM-9 TUR CW-2 KP-N-YS COLO-824 NB14 KASUMI-1 COLO-800 MRK-nu-1 HT HDLM-2 NCI-H446 SHP-77 WSU-NHL KMS-12-PE
HRASLS3
VPS24
GPRC5A
FTH1
H6PD
AGPAT2
PARP1
C6ORF60
PIK3R3
ORC2L
PPAT
SMARCA3
RUFY3
MTMR4
MAPRE2
CAMK4
ZNF43
C21ORF45
LN IC50
BI-D1870 (5.06)
60 40 20 0
TFIP11 /// LOC653715
C14ORF173
H2AFJ
SULT1A1
C7ORF10
PCYOX1
HNMT
CXORF40B
TMEM16K
CALML4
FABP1
LN IC50
RDEA119 (5.04)
60 40 20 0
skin
SPRY2
GSTO1
CENTD3
PHLDA1
C3ORF64
TRIB2
C15ORF38
C10ORF56
RET
ZNF14
ASCC3L1
TIMELESS
SAP30
DCC1
FBXO42
GADD45G
TBCC
WHSC1
LN IC50

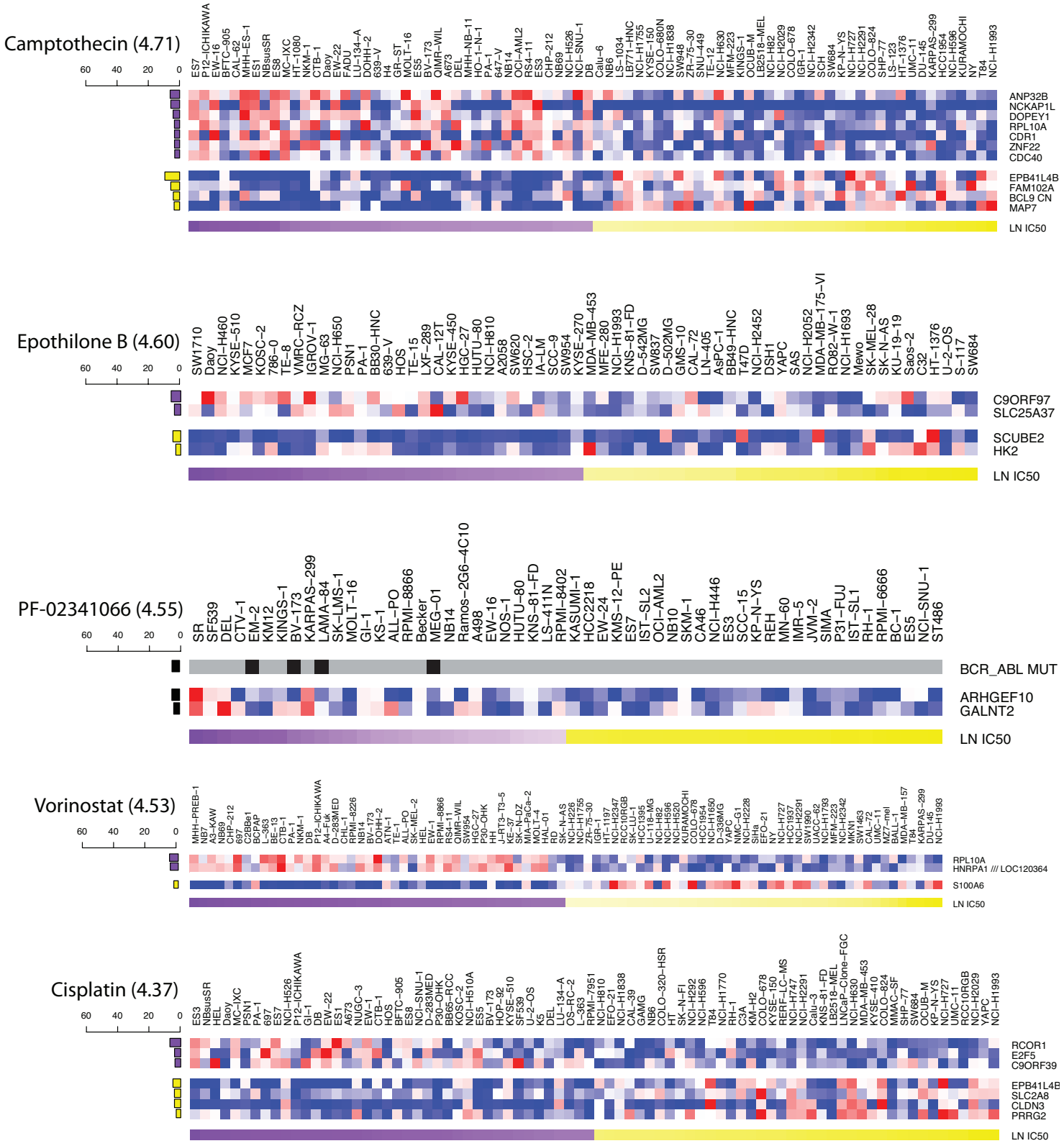
Camptothecin (4.71)
60 40 20 0
ES7 P12-ICHIKAWA EW-16 BFTC-905 CAL-62 MHH-ES-1 ES1 NBsusSR ES8 MC-IXC HT-1080 NKM-1 CTB-1 Daoy EW-22 FADU LU-134-A DOHH-2 639-V H4 GR-ST MOLT-16 ES5 BV-173 OIMR-WIL A673 DEL MHH-NB-11 HO-1-N-1 PA-1 647-V NB14 OCI-AML2 RS4-11 ES3 CHP-212 NB69 NCI-H526 NCI-SNU-1 DB Calu-6 NB6 LS-1034 LB771-HNC NCI-H1755 KYSE-150 COLO-680N NCI-H1838 SW948 SNU-75-30 SNU-449 TE-11 NCI-H630 MFM-223 KINGS-1 OCUBE-M LB2518-MEL NCI-H82 NCI-H2029 COLO-678 IGR-1 NCI-H2342 SW684 SW1990 KP-N-YS NCI-H727 NCI-H2291 COLO-824 SHP-77 S-123 HT-1376 UMC-11 DU-145 KARPAS-299 NCI-H596 KURAMOCHI NY T84 NCI-H1993
ANP32B
NCKAP1L
DOPEY1
RPL10A
CDR1
ZNF22
CDC40
EPB41L4B
FAM102A
BCL9 CN
MAP7
LN IC50
Epothilone B (4.60)
60 40 20 0
SW1710 Daoy NCI-H460 KYSE-510 MCF7 KOSC-2 786-0 TE-8 VMRC-RCZ IGROV-1 MG-63 NCI-H650 PSN1 PA-1 BB30-HNC 639-V HOS TE-15 LXF-289 CAL-12T KYSE-450 HGC-27 HUTU-80 NCI-H810 A2058 SW620 HSC-2 IA-LM SCC-9 SW954 KYSE-270 MDA-MB-453 MFE-280 NCI-H1993 KNS-81-FD D-542MG SW837 D-502MG GMS-10 CAL-72 LN-405 AsPC-1 BB49-HNC T47D NCI-H2452 DSH1 YAPC SAS NCI-H2052 MDA-MB-175-VI RO82-W-1 NCI-H1693 Mewo SK-MEL-28 SK-N-AS KU-19-19 Saos-2 C32 HT-1376 U-2-OS S-117 SW684
C9ORF97
SLC25A37
SCUBE2
HK2
LN IC50
PF-02341066 (4.55)
60 40 20 0
SR SF539 DEL CTV-1 EM-2 KM12 KINGS-1 BV-173 KARPAS-299 LAMA-84 SK-LMS-1 MOLT-16 GI-1 KS-1 ALL-PO RPMI-8866 Becker MEG-01 NB14 Ramos-2G6-4C10 A498 EW-16 NOS-1 HUTU-80 KNS-81-FD LS-411N RPMI-8402 KASUMI-1 HCC2218 EW-24 KMS-12-PE ES7 IST-SL2 OCI-AML2 NB10 SKM-1 CA46 NCI-H446 ES3 SCC-15 KP-N-YS REH MN-60 IMR-5 JVM-2 SIMA P31-FUJ IST-SL1 RH-1 RPMI-6666 BC-1 ES5 NCI-SNU-1 ST486
BCR_ABL MUT
ARHGEF10
GALNT2
LN IC50
Vorinostat (4.53)
60 40 20 0
MHH-PREB-1 NB7 A3-KAW NB69 CHP-212 697 BCPAP EPP1 L-363 BE-13 CTB-1 PA-1 NKM-1 PB P12-ICHIKAWA A4-Fuk D-283MED CHL-1 RPMI-8226 NB14 BV-173 OCI-H1-2 ATN-1 TE-1 ALL-PO SK-MEL-2 HEL EW-1 RPMI-8866 A673 OIMR-WIL SW954 HGC-27 P30-OHK HH J-RT3-T3-5 KE-37 SK-N-DZ MIA-PaCa-2 MOLT-4 HAL-01 RD SK-N-AS NCI-H226 NCI-H1755 ZR-75-30 IGR-1 HT-1197 NCI-H2347 RCC10RGB SK-LU-1 HCC1395 NCI-H146 NCI-H82 NCI-H596 NCI-H520 KURAMOCHI COLO-678 HCC1954 NCI-H650 D-342MG YAPC NMC-G1 NCI-H2228 SiHa EFO-21 NY NCI-H727 HCC1937 NCI-H2291 SW1990 UACC-62 NCI-H1793 MFM-223 NCI-H2342 NY SW1463 CAL-72 UMC-11 MZ7-mel BALL-1 MDA-MB-157 T84 KARPAS-299 DU-145 NCI-H1993
RPL10A
HNRPA1 /// LOC120364
S100A6
LN IC50
Cisplatin (4.37)
60 40 20 0
ES3 NBsusSR HEL Daoy MC-IXC PSN1 PA-1 697 ES7 NCI-H526 P12-ICHIKAWA GI-1 DB EW-22 ES1 A673 NUGC-3 EW-1 CTB-1 HOS ES8 BFTC-905 NCI-SNU-1 D-283MED P30-OHK BB65-RCC KOSC-2 NCI-H510A ES5 BV-173 HOP-92 KYSE-510 SF539 U-2-OS K5 DEL LU-134-A OS-RC-2 L-363 RPMI-7951 NCI-H810 EFO-21 NCI-H1838 CAL-39 GAMG NB6 COLO-320-HSR HT SK-N-FI NCI-H292 NCI-H596 T84 NCI-H1770 RH-1 C3A KM-H2 COLO-678 KYSE-150 RERF-LC-MS NCI-H747 NCI-H2291 Calu-3 KNS-81-FD LB2518-MEL LNCaP-Clone-FGC NCI-H630 MDA-MB-453 KYSE-410 COLO-824 MMAC-SF SHP-77 SW684 OCUB-M KP-N-YS NCI-H727 UMC-11 RCC10RGB NCI-H2029 YAPC NCI-H1993
RCOR1
E2F5
C9ORF39
EPB41L4B
SLC2A8
CLDN3
PRRG2
LN IC50

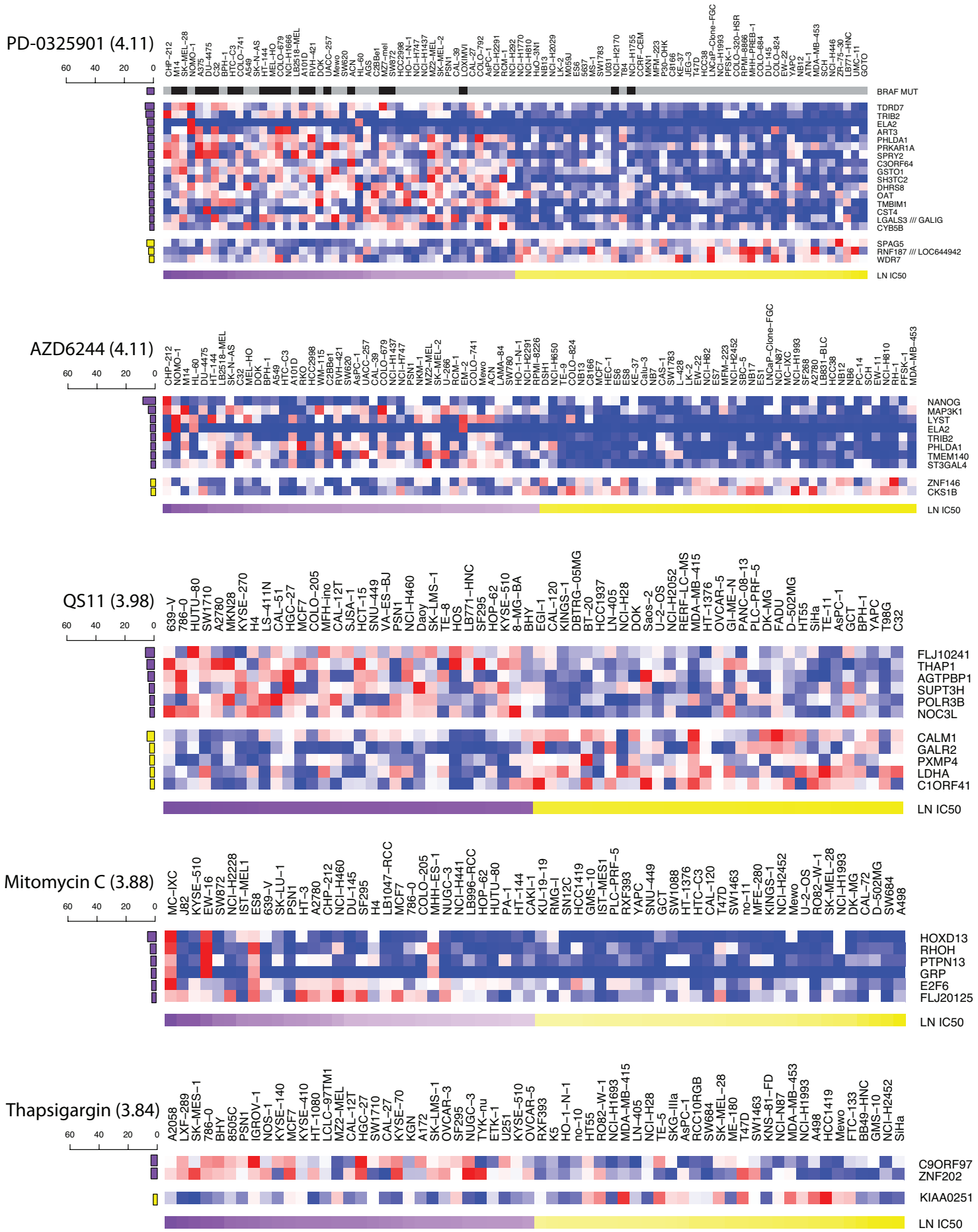
PD-0325901 (4.11)
60 40 20 0
CHP–212 M14 SK–MEL–28 NOMO–1 A375 DU–4475 C32 BPH–1 HTC–C3 COLO–741 A549 SK–N–AS LE–1–41 MEL–HO COLO–679 NCI–H1666 LB2518–MEL A101D RVH–421 DOK HCC–257 Mewo SW620 ACN HL–60 AGS C2BBe1 MZ7–mel SW872 HCC2998 HO–1–N–1 NCI–H747 NCI–H1437 MZ2–MEL SK–MEL–2 PSN1 CAL–39 LOXIMVI CAL–27 COLO–792 AsPC–1 NCI–H2291 RCM–1 NCI–H292 NCI–H1770 NCI–H810 HuO–3N1 NB13 NCI–H2029 KYSE–2 MDA–MB–231 SW1783 U031 NCI–H2170 T98G NCI–H1755 CCRF–CEM MKN1 MFM–223 P30–OHK C8166 KE–37 JEG–3 T47D HCC38 LNCaP–Clone–FGC NCI–H1993 PFSK–1 COLO–320–HSR RPMI–8866 MIH–PREB–1 COLO–684 DU–145 COLO–824 EW–22 NB4 NBT–C ATN–1 MDA–MB–453 SCH NCI–H446 ZR–75–30 LB771–HNC NCI–H211 GOTO
BRAF MUT
TDRD7
TRIB2
ELA2
ART3
PHLDA1
PRKAR1A
SPRY2
C3ORF64
GSTO1
SH3TC2
DHRS8
OAT
TMBIM1
CST4
LGALS3 /// GALIG
CYB5B
SPAG5
RNF187 /// LOC644942
WDR7
LN IC50
AZD6244 (4.11)
60 40 20 0
CHP–212 NOMO–1 M14 HL–60 DU–4475 HT–144 LB2518–MEL SK–N–AS C32 MEL–HO DOK BPH–1 A549 HTC–C3 A101D RKO HCC2998 WM–115 RVH–421 SW620 AsPC–1 HCC–257 CAC–39 COLO–679 NCI–H1437 NCI–H747 PSN1 NKM–1 MZ2–MEL SK–MEL–2 U–266 RCM–1 EM–2 COLO–741 Mewo ACN LAMA–84 SW780 HO–1–N–1 NCI–H2291 RPMI–8226 DSH1 NCI–H650 TE–9 COLO–824 NB13 C8166 MCF7 HEC–1 ES6 ES8 KE–37 Calu–3 NB7 CAS–1 SW1783 L–428 LK–2 EW–22 NCI–H82 ES7 MFM–223 NCI–H2452 SBC–5 NB17 ES1 LNCaP–Clone–FGC NCI–N87 MC–IXC NCI–H1993 SF268 A2780 LB831–BLC HCC38 NB12 NB6 PC–14 SCH EW–11 NCI–H810 RH–1 PFSK–1 MDA–MB–453
NANOG
MAP3K1
LYST
ELA2
TRIB2
PHLDA1
TMEM140
ST3GAL4
ZNF146
CKS1B
LN IC50
QS11 (3.98)
60 40 20 0
639–V 786–0 HUTU–80 SW1710 A2780 MKN28 KYSE–270 H4 LS–411N CAL–51 HGC–27 MCF7 COLO–205 MFH–ino CAL–12T SJSA–1 HCT–15 SNU–449 VA–ES–BJ PSN1 NCI–H460 Daoy SK–LMS–1 TE–8 HOS LB771–HNC SF295 HOP–62 KYSE–510 8–MG–BA BHY EGI–1 CAL–120 KINGS–1 DBTRG–05MG BT–20 HCC1937 LN–405 NCI–H28 DOK Saos–2 U–2–OS NCI–H2052 RERF–LC–MS MDA–MB–415 HT–1376 OVCAR–5 GI–ME–N PANC–08–13 PLC–PRF–5 DK–MG FADU D–502MG HT55 SiHa TE–11 AsPC–1 GCT BPH–1 YAPC T98G C32
FLJ10241
THAP1
AGTPBP1
SUPT3H
POLR3B
NOC3L
CALM1
GALR2
PXMP4
LDHA
C1ORF41
LN IC50
Mitomycin C (3.88)
60 40 20 0
MC–IXC J82 KYSE–510 EW–16 SW872 NCI–H2228 IST–MEL1 ES8 639–V SK–LU–1 PSN1 HT–3 A2780 CHP–212 NCI–H460 DU–145 SF295 H4 LB1047–RCC MCF7 786–0 COLO–205 MHH–ES–1 NUGC–3 NCI–H441 LB996–RCC HOP–62 HUTU–80 PA–1 HT–144 CAKI–1 KU–19–19 RMG–I SN12C HCC1419 GMS–10 IST–MES1 PLC–PRF–5 RXF393 YAPC SNU–449 GCT SW1088 HT–1376 HTC–C3 CAL–120 T47D SW1463 no–11 MFE–280 KINGS–1 NCI–H2452 Mewo U–2–OS RO82–W–1 SK–MEL–28 NCI–H1993 DK–MG CAL–72 D–502MG SW684 A498
HOXD13
RHOH
PTPN13
GRP
E2F6
FLJ20125
LN IC50
Thapsigargin (3.84)
60 40 20 0
A2058 LXF–289 SK–MES–1 786–0 BHY 8505C PSN1 IGROV–1 NOS–1 KYSE–140 MCF7 KYSE–410 HT–1080 LCLC–97TM1 MZ2–MEL CAL–12T HGC–27 SW1710 CAL–27 KYSE–70 KGN A172 SK–LMS–1 OVCAR–3 SF295 NUGC–3 TYK–nu ETK–1 U251 KYSE–510 OVCAR–5 RXF393 K5 HO–1–N–1 no–10 HT55 RO82–W–1 NCI–H1693 MDA–MB–415 LN–405 NCI–H28 TE–5 SKG–IIIa AsPC–1 RCC10RGB SW684 SK–MEL–28 ME–180 T47D SW1463 KNS–81–FD NCI–N87 MDA–MB–453 NCI–H1993 A498 HCC1419 Mewo FTC–133 BB49–HNC GMS–10 NCI–H2452 SiHa
C9ORF97
ZNF202
KIAA0251
LN IC50

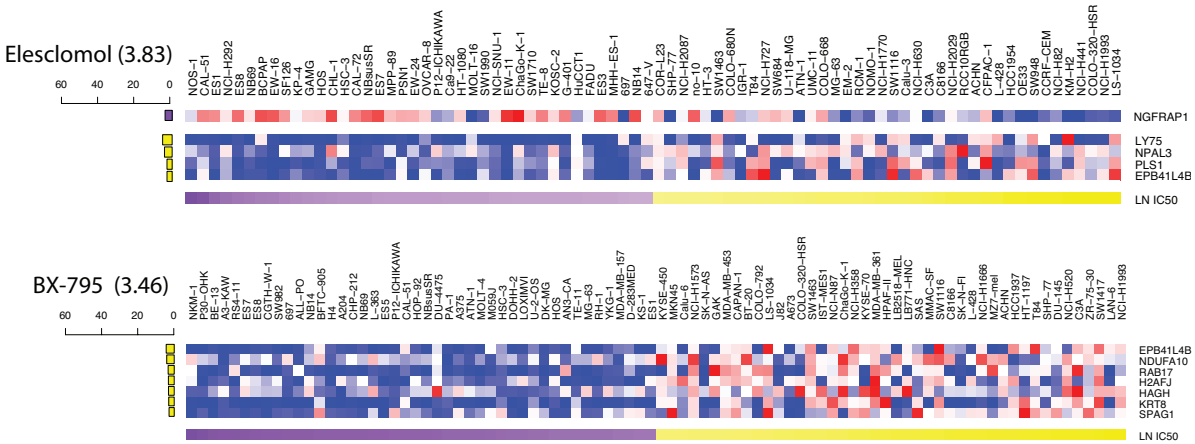

Supplementary Figure 13: Heatmaps for features in marker signatures of all drugs that have at least 2 features with significant effect sizes (-2.95>e>2.79). Only features with significant effect sizes are shown. Mutation and tissue features are at the top of the heatmap shown in black (sample has feature) and gray (sample lacks feature) followed by sensitivity associated expression and copy number features and finally resistance associated expression and copy number features. To the left of each feature is a barplot indicating the absolute value of the effect size. Bars in purple are negative effects, indicating features associated with sensitivity and bars in yellow are positive effects, indicating features associated with resistance. The natural log IC50 for each cell line is represented at the bottom. Cell lines shown for each heatmap are those with lowest and highest 10% of IC50s for each drug.

Resistance				
Genes	Drug	Target	Frequency	Effect
TP53 MUT	**Nutlin-3a**	MDM2	1	60.57
BIN2	**Vinorelbine**	Microtubules	0.95	53.19
ZNF643	**MG-132**	Proteasome	1	21.95
RIMBP2	**JW-7-52-1**	MTOR	1	21.17
	Paclitaxel	Microtubules	1	13.32
	GW843682X	PLK1	0.99	7.34
ABCB1	**Docetaxel**	Microtubules	1	20.89
	Vinblastine	Microtubules	1	12.91
	Vinorelbine	Microtubules	1	11.40
	17-AAG	HSP90	1	4.62
ZNF467	**GW843682X**	PLK1	0.99	19.48
	Paclitaxel	Microtubules	1	14.17
	BI-2536	PLK1/2/3	0.85	8.23
RB1 MUT	**PD-0332991**	CDK4/6	1	18.10
EPB41L4B	**PD-0332991**	CDK4/6	1	17.34
	Temsirolimus	MTOR	1	10.00
	Camptothecin	TOP1	1	9.48
	CEP-701	FLT3, JAK2, NTRK1, RET	1	8.43
	NVP-BEZ235	PI3K /mTor	0.97	8.35
	Cisplatin	DNA crosslinker	1	5.00
	BX-795	TBK1, PDK1, IKK, AURKB/C	1	4.44
	Elesclomol	HSP70	1	2.85
C1ORF109	**Z-LLNle-CHO**	g-secretase	1	16.09
CCNT2	**Dasatinib**	ABL, SRC, KIT, PDGFR	1	15.96
GARNL1	**MG-132**	Proteasome	1	14.91
PLAGL2	**17-AAG**	HSP90	1	13.14

Sensitivity				
Gene	Drug	Target	Frequency	Effect
BCR_ABL MUT	**Dasatinib**	ABL, SRC, KIT, PDGFR	1	-61.29
	Nilotinib	ABL	1	-52.42
	WH-4-023	SRC, ABL	0.99	-43.69
	Imatinib	ABL, KIT, PDGFR	1	-28.72
	GNF-2	BCR-ABL	1	-22.63
	AZD-0530	SRC, ABL	1	-15.34
	PF-02341066	MET, ALK	0.99	-4.88
	Axitinib	PDGFR, KIT, VEGFR	1	-3.37
LAG3	**GSK-650394**	SGK3	1	-29.90
MMP28	**Lapatinib**	EGFR, ERBB2	1	-27.54
	WZ-1-84	BMX	1	-12.54
ERBB2	**Lapatinib**	EGFR, ERBB2	1	-26.41
	BIBW2992	EGFR, ERBB2	1	-9.34
PERLD1	**Lapatinib**	EGFR, ERBB2	1	-23.70
BRAF MUT	**PLX4720**	BRAF	1	-23.25
	SB590885	BRAF	1	-7.89
	PD-0325901	MEK1/2	1	-4.99
NQO1	**17-AAG**	HSP90	1	-22.21
ADK	**AICAR**	AMPK agonist	1	-21.52
CDKN2a(p14) MUT	**Dasatinib**	ABL, SRC, KIT, PDGFR	1	-20.28
	WH-4-023	SRC, ABL	0.99	-11.93
PCSK5	**Erlotinib**	EGFR	1	-19.60
TRIM16	Dasatinib	ABL, SRC, KIT, PDGFR	1	-19.27
	AZD-0530	SRC, ABL	1	-3.52

Supplementary Table 3: Highly significant genomic biomarkers of drug response from EN analysis. High frequency features (f > 0.76) associated with the largest effect sizes are displayed together with the relevant drug and grouped into positive effect sizes associated with resistance (left) and negative effect sizes associated with sensitivity (right). The top 15 resistance and sensitivity associations are in bold and additional drugs that are associated with each gene at the significance criteria are included in the table.

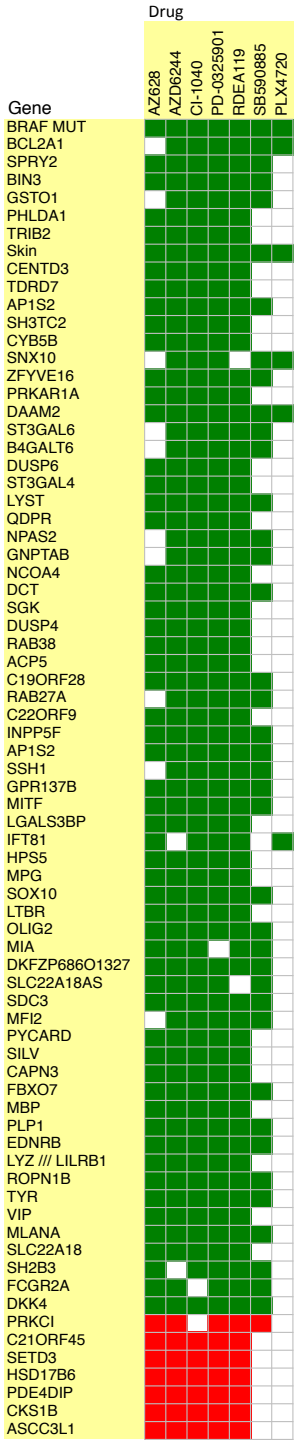

Supplementary Figure 14: Heatmap of recurrent features in RAF and MEK1/2 inhibitor signatures from EN analysis. Green indicates that the feature is associated with drug sensitivity and red indicates association with resistance. Features displayed were present in 5 or more of the 7 RAF and MEK1/2 inhibitors screened.

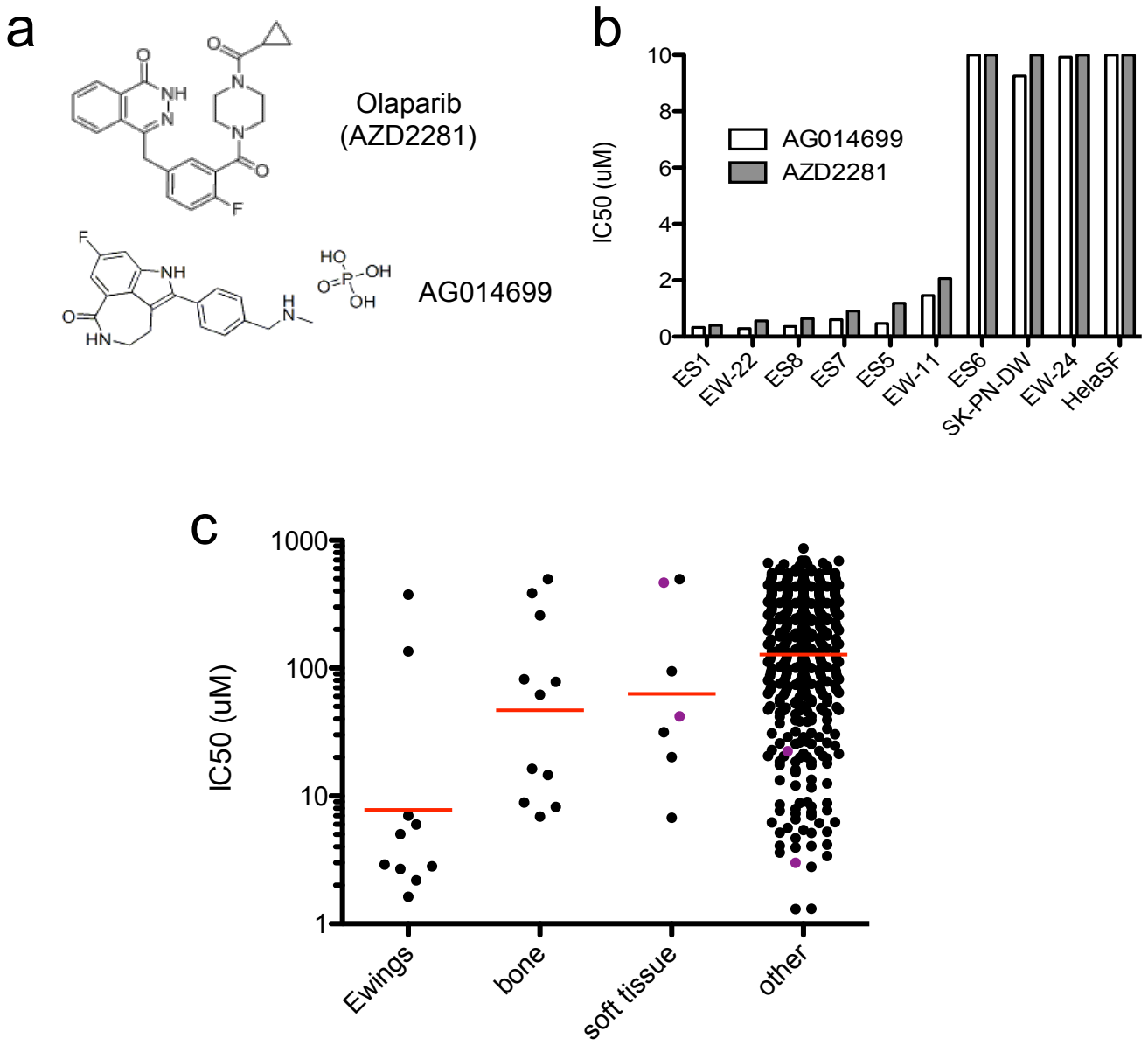

Supplementary Figure 15: Ewing's sarcoma cells are sensitive to multiple PARP inhibitors. a, Chemical structures of PARP inhibitors olaparib and AG014699 used in this study. **b**, Comparison of IC_{50} values of Ewing's cells to olaparib and AG014699 in a 6-day viability assay. IC_{50} values are capped at 10 uM and HeLaSF cells are included as a negative control. The majority of Ewing's sarcoma cells are acutely sensitive to PARP inhibitors but some cells to do not respond in this assay. **c,** Ewing's sarcoma cells show marked sensitivity to olaparib compared to other bone and soft tissue cancers. A scatter plot of cell line IC_{50} values (n = 459) to olaparib on a log scale is shown and the red line indicates the geometric mean. Purple circles are cell lines which have the *EWS-FLI1* rearrangement but historically have not been classified histologically as Ewing's.

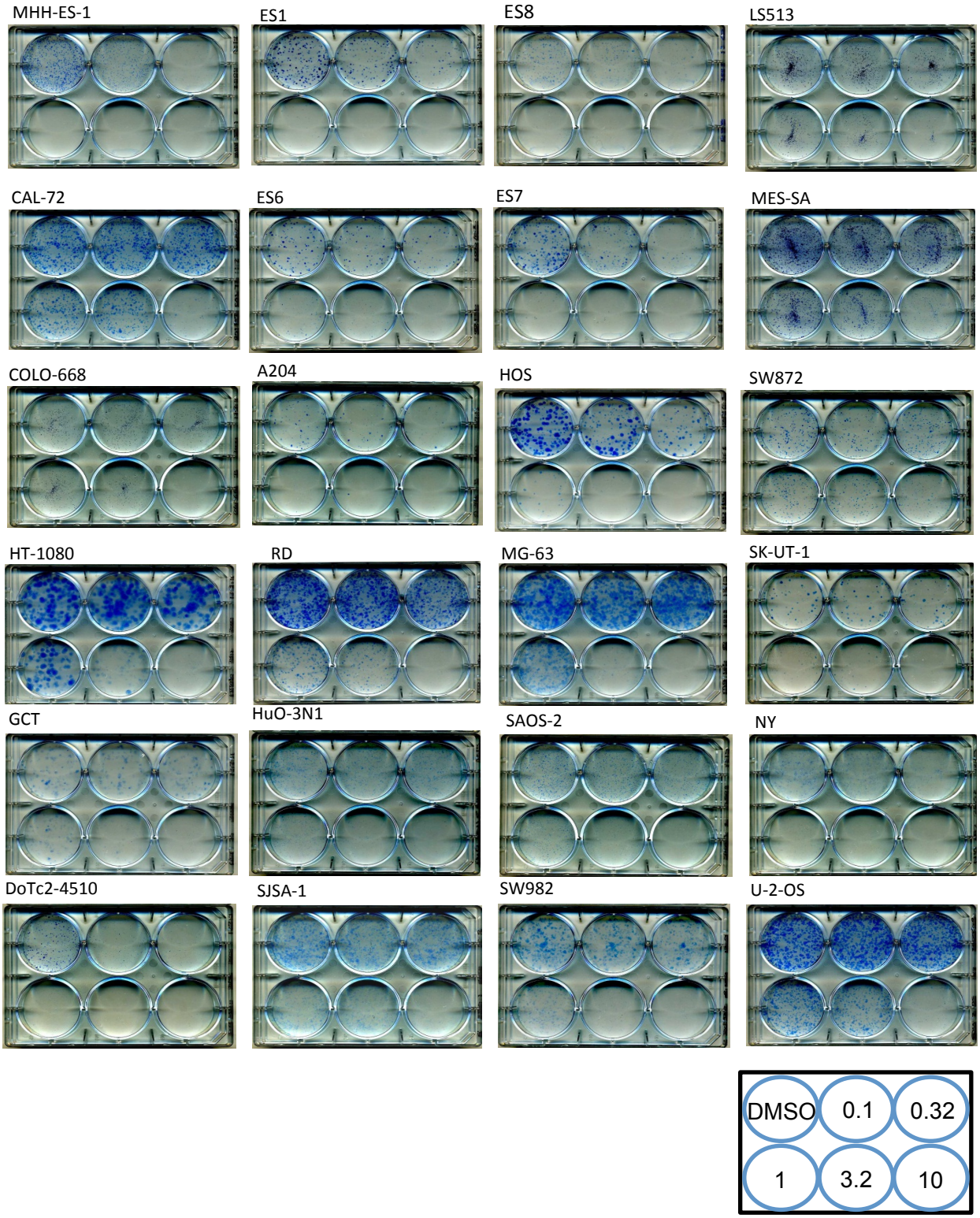

Supplementary Figure 16: Images of olaparib clonogenic assays for Ewing's sarcoma and control cell lines. Clonogenic assays were performed in the presence of increasing concentrations of olaparib (0.1, 0.32, 1, 3.2 or 10 uM final concentration). Plates were re-drugged every 4 days and fixed and stained 7-21 days following plating. The name of each cell line is given and a schematic (lower right) shows the concentration used for each well.

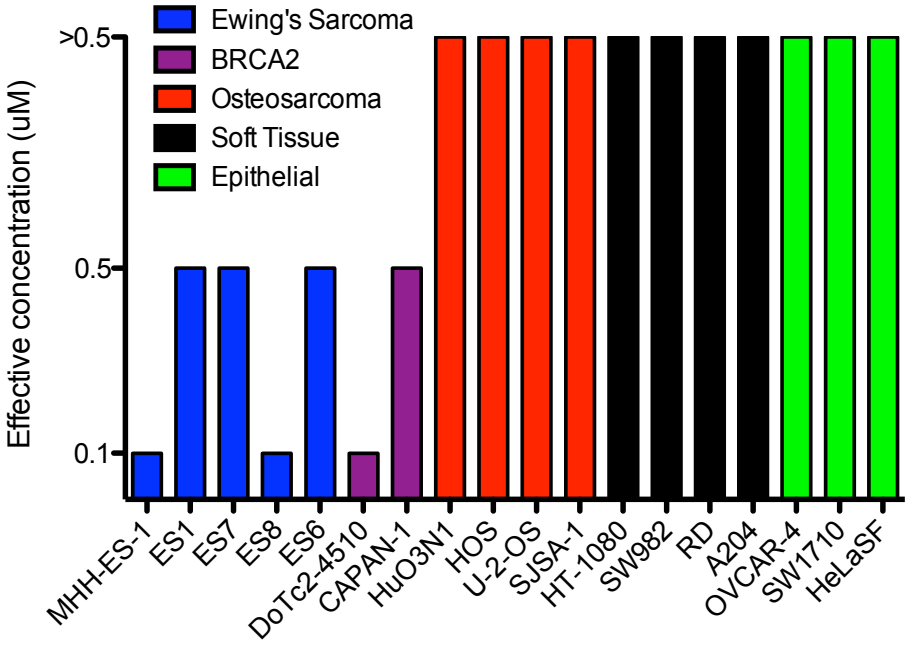

Supplementary Figure 17: Ewing's sarcoma cells are sensitive to PARP inhibitor AG014699 in colony formation assays. Cell lines were treated with 0.1 uM or 0.5 uM AG014699 for 7-21 days with re-drugging every 3-4 days. For each cell line the concentration necessary to reduce colonies >90% relative to controls is plotted.

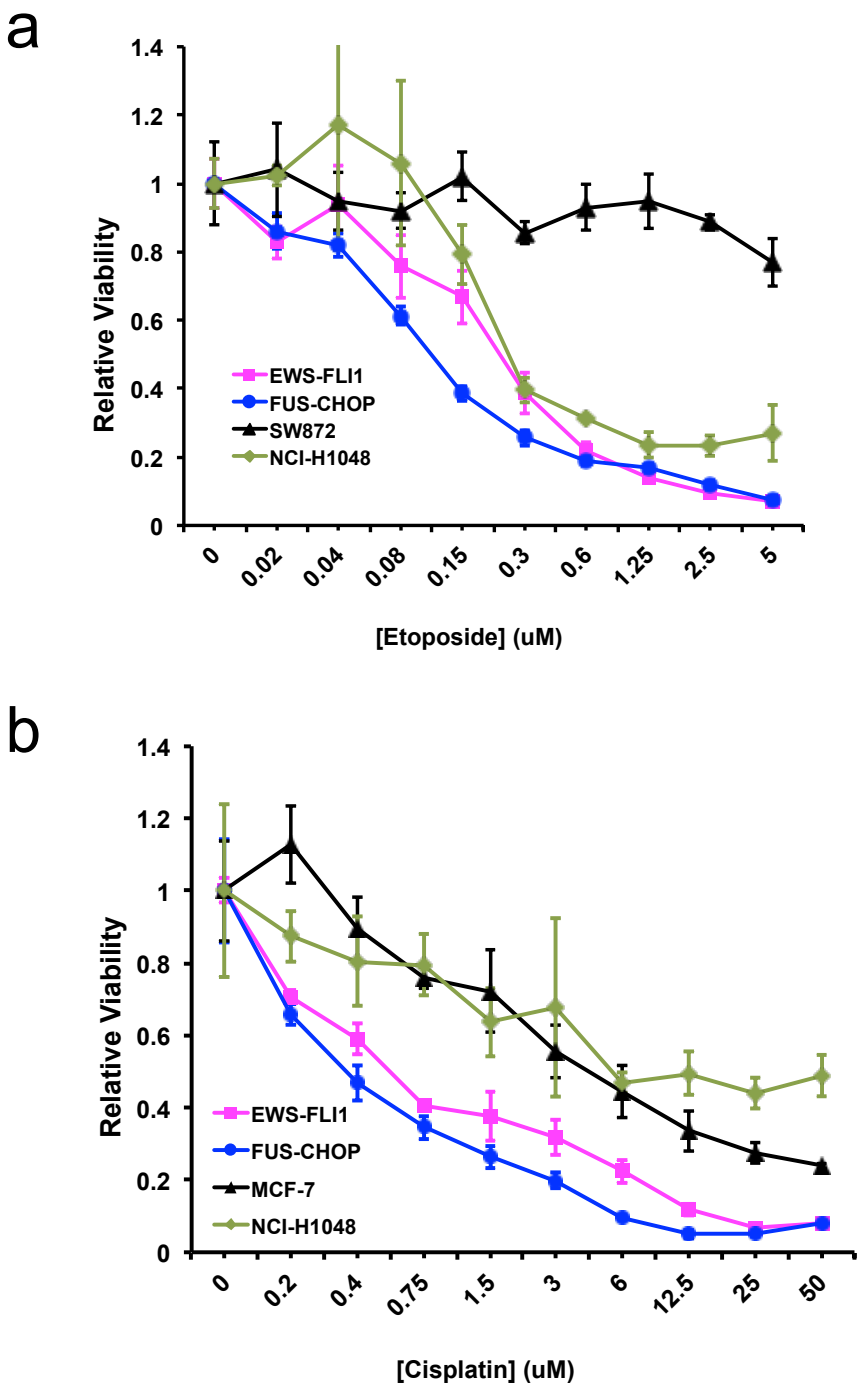

Supplementary Figure 18: *EWS-FLI1* transformed mouse mesenchymal cells are not sensitised to etoposide or cisplatin. As a control we show dose response curves to **a**, etoposide or **b,** cisplatin comparing the sensitivity of *EWS-FLI1* and *FUS-CHOP* transformed mouse mesenchymal cells. Human non-mesenchymal cell lines were included as an additional control. Each drug concentration was assayed in triplicate and error bars represent s.d.

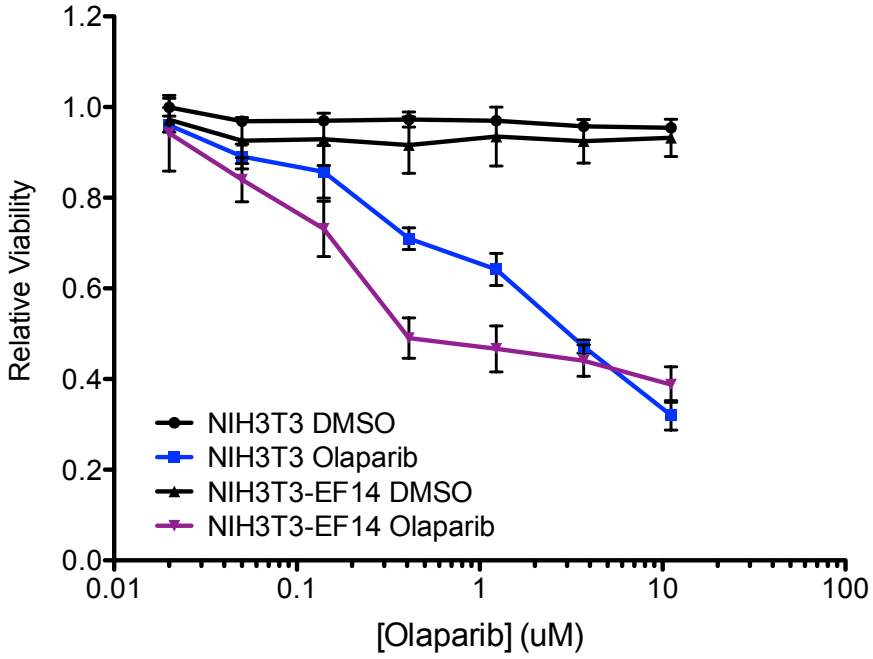

Supplementary Figure 19: EWS-FLI1 expression is specifically associated with PARP inhibitor sensitivity. Olaparib dose response curves of NIH3T3 cells stably expressing EWS-FLI1 (NIH3T3-EF14) or the parental control line. Expression of EWS-FLI1 increased sensitivity to olaparib. The effect was greatest at low doses of olaparib whereas at higher doses both cell lines were sensitive presumably due to general cellular toxicity. Viability was normalised to untreated cells. Each drug concentration was assayed in triplicate and error bars represent the s.d.

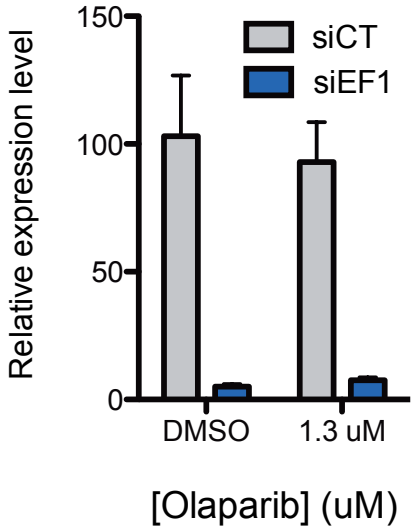

Supplementary Figure 20: Confirmation of siRNA-mediated depletion of EWS-FLI1 in A673 cells. A673 were transfected with either control (siCT) or EWS-FLI1 (siEF1) siRNA for 72 hours and cells were concomitantly treated with either olaparib or DMSO. Relative expression levels of EWS-FLI1 (normalized to ribosomal protein RPLP0) were assessed by RT-QPCR. Expression was assayed in triplicate and errors bars are s.d.

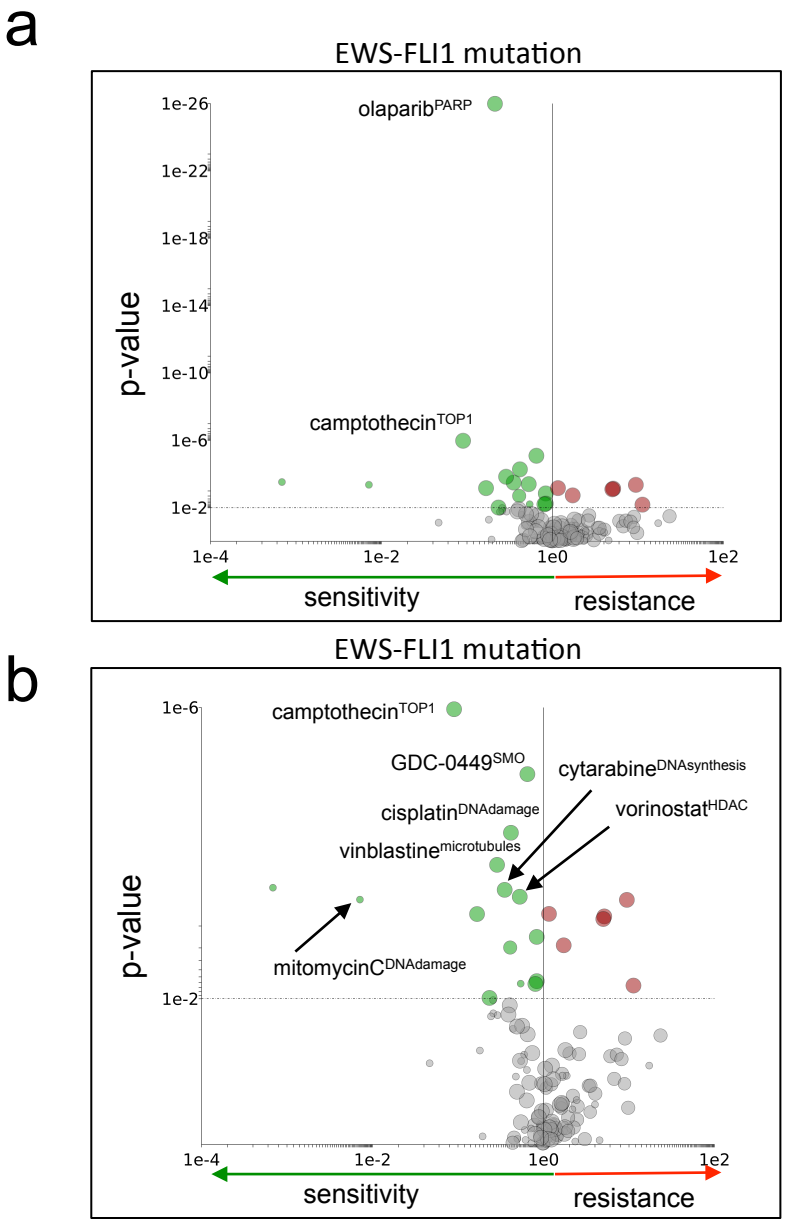

Supplementary Figure 21: The *EWS-FLI1* rearrangement is associated with sensitivity to cytotoxic drugs. **a** and **b**, *EWS-FLI1* mutation-specific volcano plots of drug sensitivity from MANOVA. The drug name is indicated and therapeutic drug target(s) (in superscript) are indicated for selected data. Circle size is proportional to the number of mutant cell lines screened (max = 14 for **a** and **b**). For **b** the data for olaparib has been removed to make less significant associations clear (note the change to scaling on y-axis).

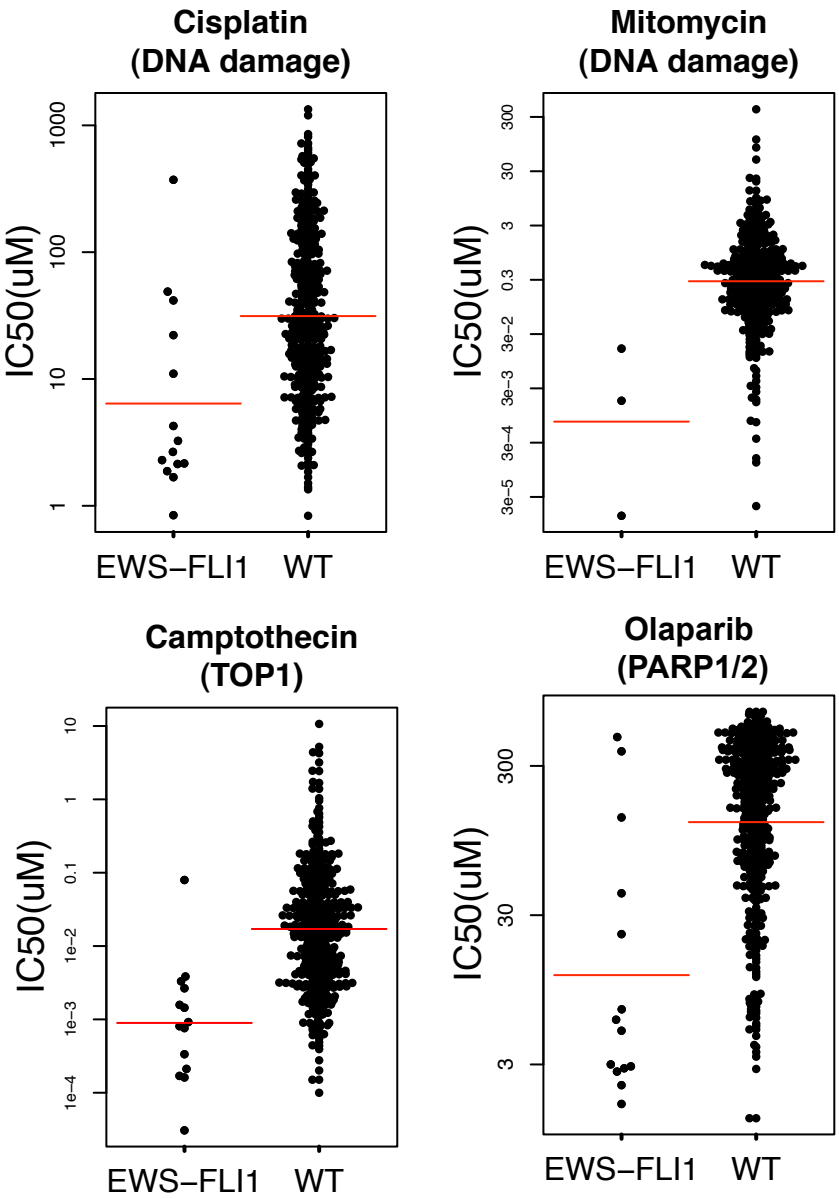

Supplementary Figure 22: **Association of the *EWS-FLI1* translocation with sensitivity to DNA damaging agents.** Scatter plots of IC_{50} values from selected associations from the MANOVA of *EWS-FLI1* with cytotoxic drugs. The data for olaparib (AZD-2281) is also included for comparison. The cell line IC_{50} values (uM) for each drug are given comparing mutated (MUT) or non-mutated (WT) cell lines. Each circle represents the IC_{50} of one cell line plotted on a log scale and the red bar is the geometric mean. The drug name is indicated above each plot and target(s) are given in brackets.